UNIVERSITY OF CALIFORNIA, SAN DIEGO

**Finite Duration Shocks on Discrete Laminate Composite Al/W**

A Thesis submitted in partial satisfaction of the
requirements for the degree
Master of Science

in

Engineering Sciences (Applied Mechanics)

by

Pedro Franco Navarro

Committee in charge:

Professor Vitali F. Nesterenko, Chair
Professor David J. Benson, Co-Chair
Professor Prabhakar R. Bandaru

2013

The Thesis of Pedro Franco Navarro is approved, and it is acceptable in quality and form for publication on microfilm and electronically:

_____

_____

Co-Chair

_____

Chair

University of California, San Diego

2013

DEDICATION

For all their support even in the hardest moments I thank my family, their inconditional love and encouragement made this possible.

# EPIGRAPH

*We all die. The goal isn't to live forever,*
*the goal is to create something that will*
—Chuck Palahniuk

*Our virtudes and our failings are inseparable,*
*like force and matter. When they separate,*
*man is no more.*
—Nikola Tesla

TABLE OF CONTENTS

LIST OF FIGURES

LIST OF TABLES

ACKNOWLEDGEMENTS

Thanks to Vitali Nesterenko and Daviv Benson for all their guidance, support and patience on this endeavor; their role has been the key stone of this project. To my loving mother Cuquita and my awesome dad Pedro, who supported me and never stopped believing in me, and to my sisters Haydeé and Ingrid who never doubted me. To my dear friends who supported me through my decision of pursuing grad school. Special thanks to Ing. Eugenio Clariond, CONACYT and the von Liebig Center for their support and for believing in the next generation of Mexican scientists, and finally to the fellows at P360, who helped me to regain my coinfidence, which started to drop near the end of this endeavor.

Chapters 2,3,4,5 and 6, partially, are to be used in a subsequent publication. The thesis author is going to be the primary investigator and author of this paper.

## VITA

| | |
|---|---|
| 2009 | B. S. in Mechatronics Engineering, Instituto Tecnológico y de Estudios Superiores de Monterrey, Monterrey, Mexico. |
| 2010 | Mechanical Design Engineer, Honeywell Aerospace, Mexicali, Mexico. |
| 2011 | Mechanical Design Engineer, PACCAR Inc, Mexicali Mexico. |
| 2013 | M. S. in Engineering Sciences (Mechanical Engineering), University of California, San Diego. |

## FIELDS OF STUDY

Major Field: Engineering Sciences (Applied Mechanics)

Areas of Specialization: Solid Mechanics, Numerical Methods and Finite Element

ABSTRACT OF THE THESIS

**Finite Duration Shocks on Discrete Laminate Composite Al/W**

by

Pedro Franco Navarro

Master of Science in Engineering Sciences (Applied Mechanics)

University of California, San Diego, 2013

Professor Vitali F. Nesterenko, Chair
Professor David J. Benson, Co-Chair

Numerical simulations of strong shock wave compression of Al-W laminate materials with different cell size ranging from 1 mm to 4 mm were conducted. Finite element simulations using LS-DYNA were employed with two different durations of loading pulse tailored by changing the length of the impactor. The results of the numerical simulations for homogeneous materials were used for validation of our code by comparing the results of the pressure, the temperature and the final volume with the available Hugoniot data.

The focus of this work was on the study of the mechanical parameters and thermodynamic states reached through multiple shock reverberations. The mechanism of the formation of the steady leading front and final states were analyzed

under different conditions of loading and laminate mesostructure. It was shown that a steady shock front can be reached even when the final steady state is not established. The results of the numerical simulations of the pressure, the specific volume and the temperature were compared to the values predicted by two models to assess whether these models correctly predict the final state. This work also includes a brief exploration of the effects of mesh refinement and shock viscosity on the simulated final state of the material.

It is concluded that an increasing number of interfaces (through the reduction of the layer thicknesses) helps to achieve a steady shape of the leading front and the equilibrium state behind the shock faster. The investigated models correctly predict the final state (within the explored ranges of pressure) in the pressure-specific volume plane. It was also found that the final thermodynamic state is more sensitive to the composition of the layered materials and that the predictions of the models differ from our calculations even when a steady state behind the shock was reached.

# Chapter 1

# Introduction

Composite materials can be found in nature. Wood is a perfect example, where millions of fibers comprise a material that has good mechanical properties and it has been at the disposal of humanity for generations. During the last 100 years better materials that offer much better mechanical properties without sacrificing performance were developed, including layered materials (LM). The understanding of the behavior of these materials under the presence of shock loading is of special interest due to particular behaviors that have been documented (Nesterenko et al., 1983; Petel et al., 2011; Benson and Nesterenko, 2001) such as the mitigation of the wave front.

This work first presents a review of previous results in the shock physics field, then it focuses on the modeling of a layered composite using LS-DYNA and to assure the fidelity of these models with known data.

Next models for homogeneous materials are presented with an emphasis on describing the final equilibrium state of the material behind the shock.

These models were used in subsequent numerical calculations. The relevant results are presented related to the shock wave structure in laminates with different cell size. Special attention was paid to the scaling of the length of the oscillatory part of the shock with the size of the layers. A steady state behind the traveling shock was identified in numerical calculations and compared with the predictions of the Hugoniot models.

It is concluded that the traveling shocks in layered composites are charac-

terized by a long time and depth to establish a steady state. It was found that the thermodynamic approaches explored are more sensitive to the final state than their pressure and specific volume counterparts.

# Chapter 2

# Background

The structure of a shock wave traveling inside a material has been an area of extensive study that flourished during the 1960s (Isbell, 2005) when the technology to measure the structure of high intensity waves became available and a great deal of effort was dedicated to the development of nuclear weapons and conventional munitions. New tools were developed to describe the behavior of materials at high pressures and high strain rates including equations of state, phase transitions, etc. Much of the data collected through the years, such as the Hugoniot curves for diverse materials, can be found in (Marsh, 1980).

As the development of materials continued, the need to understand the behavior of shock waves in composite materials, due to their unique mechanical properties, became important. In specific, laminar materials (LM), which can be used to mitigate impact and blast loading, have received special attention in the last 60 years. Their applications are not restricted to the military environment; they are also widely used in aerospace application, where space vehicles might suffer high velocity impacts from space debris or meteorites.

One of the first approaches to characterize LM can be found in the work of (Rytov, 1955), which determined that 5 different Lamé constans are needed to fully characterize the composite. This approximation was developed for acoustic waves, but this work is also important for strong shocks.

The main studies of strong impulses on LM focus on wave transformation. Such studies, for example, try to find the relationship that might exist between the

amplitude of the leading shock wave and the thickness of the layers that comprise the composite material in the direction of the traveling shock. As mentioned before, a wide arrange of information can be found for homogeneous materials, but since the geometry of the composite material has a big influence (later shown on Chapter 5), such compendiums do not exist for LM. The research community has produced diverse approaches aiming to predict the final state of the material. These approaches vary in complexity and exactness, and two particular ones are presented in (Petel and Jetté, 2009) as a means to predict the final pressure, specific volume and temperature once the shock loading process has taken place. These approaches assume a steady state for the traveling pressure wave. But, in a layered composite the steady state may be hard to achieve, and the shock wave propagation in finite laminates can result in peculiar and counterintuitive effects such as increase of amplitude of the wave with decrease of layer thickness which contradicts the behavior based on difference of the acoustic impedances of linear elastic materials (Nesterenko et al., 1983; Nesterenko, 2001).

The dissipation processes during the shock loading determines the width of the shock wave. In homogeneous materials for strong shockwaves, the following fourth power law was established to connect relationship between strain-rate and stress behind the shock in the form $\dot{\epsilon} = \alpha\sigma^4$. This result was introduced by Grady and a thorough explanation can be found on (Grady, 2010). This fourth power law has been widely adopted in the shock physics community. Nevertheless in (Zhuang et al., 2003), it can be found that such law does not apply to LM and the corresponding relation changes to a second power law, i.e. $\dot{\epsilon} = \alpha\sigma^2$. We used data presented in (Grady, 2010) to select an appropriate viscosity which will give us a correct shock width in individual materials and the correct dissipation properties in agreement with the Hugoniot calculations.

Chapter 2, partially, is to be used in a subsequent publication. The thesis author is going to be the primary investigator and author of this paper.

# Chapter 3

# Modeling

The approach taken in this work is based on modeling the layered composite using the well known commercial finite element program LS-DYNA. The data, such as the paths taken by material related to pressure, temperature and particle velocity were identified as well as the final state of the material are calculated behind the shock.

## 3.1 Geometry of the Layered Composite and Loading Conditions

LS-DYNA's capabilities allow the analysis of 3-D geometry, but we consider a laminate material with layers arranged in 1-D which is close to the existing experimental data on shock waves.

Figure 3.1 represents the geometry analyzed in our numerical modeling, where $L_c$ is the total length of the laminate composite, $L_i$ is the length of the impactor and $\Delta$X is the thickness of the layers of the periodic composite material. All layers have the same thickness. For the purposes of this study $L_c = 280$ mm for all cases. To introduce shock wave of different duration we changed value of $L_i$ from 80 to 800 mm to produce a short wave and a long wave. It is expected that the laminate structure may require a long distance to reach a steady state for the traveling wave inside the material, which can be supported by using a long

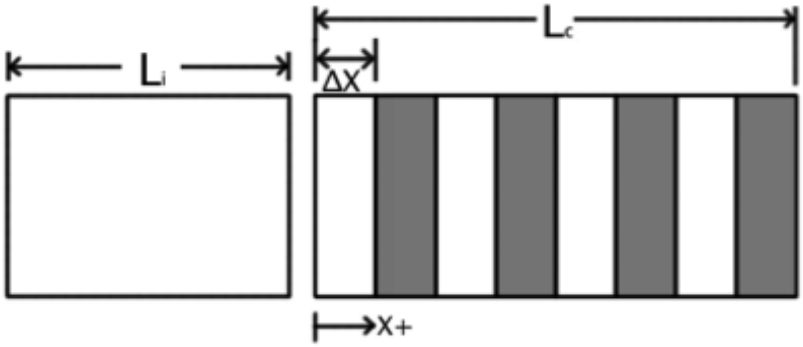


**Figure 3.1**: Layered Composite Geometry

impactor.

It is also important to establish a difference between the final shock state reached under small duration of loading provided by a short impactor. The answer to these questions depends on the thickness of layers ΔX, which ranges between .5 mm and 2 mm, thus giving cell size values ranging from one to four millimeters. Different layer thicknesses leading to a different number of interfaces may dramatically change the amplitude of the leading shock wave in laminates and affect the final states especially for small duration of shock waves even at the same length of laminate composite and similar composition (Nesterenko, 2001).

The impactor in the current study is made of aluminum and has an initial velocity of 2800 m/s in the X+ direction, while the layers of the composite are aluminum and tungsten respectively. In all cases, the layers of the composite are perfectly bonded and the end of the composite is free. It is expected that for the resulting strong shock waves at this velocity of the impactor the bonding between layers is not significant with respect to the shock wave structure and the properties of the final state. We did not consider any scenarios with tensile stresses, e.g., spall phenomena, at this stage of our research.

The mesh size was .083 mm for 1 mm cell, 0.16mm for 2 mm cell and 0.25 for the 4 mm cell. To investigate the influence of the mesh size and the viscosity, the values were reduced to get a shock front width that is around 10 times smaller than the 0.5mm layer size. Some examples of the calculations are presented to

demonstrate that the reduction of mesh size and the viscosity does not change the final states in laminates.

## 3.2 Modeling of the Shock Phenomena

The numerical solution for the shock propagation phenomena is obtained using LS-DYNA. The element size in the model changes according to $\Delta$X. Each element is composed of only one material. Both the aluminum and tungsten were modeled using the Steinberg-Guinan plasticity model (Steinberg et al., 1979) and the Grüneisen equation of state, which are available on LS-DYNA, and their implementation is described in the theory manual (Hallquist, 2006) as well as in the users manual (Livermore Software Technology Corporation, 2012a,b). The parameters for the materials are presented in Table 3.1 and were taken from (Steinberg, 1996) (with unit conversion), with the exception of the Debye temperature obtained from (Kinslow, 1970).

**Table 3.1**: Material Properties

| Parameters | Aluminum | Tungsten |
|---|---|---|
| $G_0(Pa)$ | 2.86x$10^{10}$ | 1.6x$10^{11}$ |
| $Y_0(Pa)$ | 2.6x$10^{8}$ | 2.2x$10^{9}$ |
| $\beta$ | 310 | 24 |
| n | .185 | .19 |
| $A(Pa^{-1})$ | 6.52x$10^{-11}$ | 9.38x$10^{-12}$ |
| $A'(Pa^{-1})$ | 6.52x$10^{-11}$ | 9.38x$10^{-12}$ |
| $B(K^{-1})$ | 6.16x$10^{-4}$ | 1.38x$10^{-4}$ |
| $T_{m0}$ | 1220 | 4520 |
| $C_p(\frac{Pa\ m^3}{Kg\ K})$ | 863 | 129 |
| $\Gamma_0$ | 2.00 | 1.67 |
| a | 1.5 | 1.3 |
| $\rho_0$ $(Kg/m^3)$ | 2785 | 19300 |
| $C_0(m/s)$ | 5328 | 4030 |
| $S_1$ | 1.338 | 1.237 |
| Debye $\Theta$ | 350 | 247 |

## 3.3 Shock Waves in Homogeneous Materials

First of all, it is important to validate that LS-DYNA correctly reproduces the final thermodynamic states behind shock waves based on available Hugoniot curves. It is important to show that the simulations concur with predictions of the parameters of the final state of the material (especially temperature) to prove that dissipation processes in the compression and release stages have been captured correctly.

The results of our simulations and the published Hugoniot data from (Kinslow, 1970) corresponding to a 70 GPa shock loading are presented in Figs. 3.2 and 3.3. The red points on Fig.3.2 and Fig.3.3(a) represent the final states of the material behind shock wave in Al and W and the green points shown parameters after unloading that have been obtained from LS-DYNA.

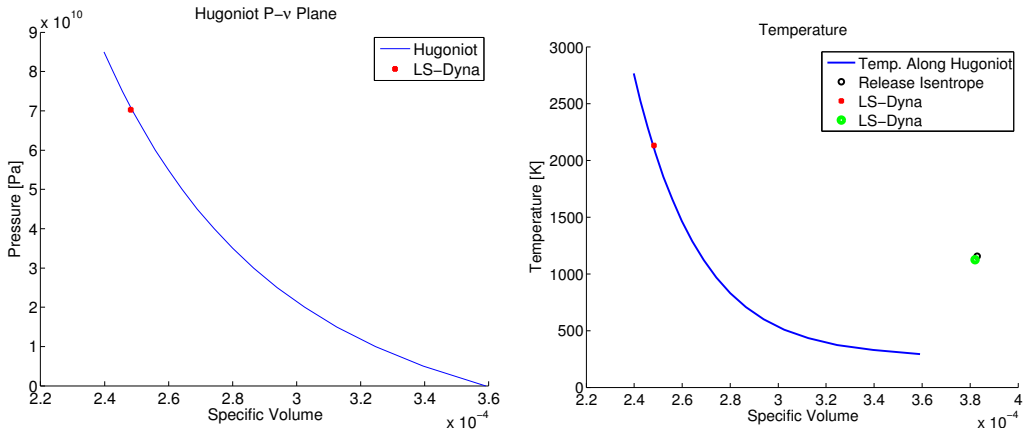


(a) (b)

**Figure 3.2**: (a) The final calculated states on the P$-\nu$ plane agree with Hugoniot data obtained from (Kinslow, 1970) (b) Final temperature of the simulation on both loading (red dot) and unloading process (green dot) match up data from (Kinslow, 1970) for pure Aluminum.

The comparison clearly shows that the used model correctly predicts the pressure and specific volume evolution in the simulation of single shock in individual materials. Even more important is that the simulations correctly predict the

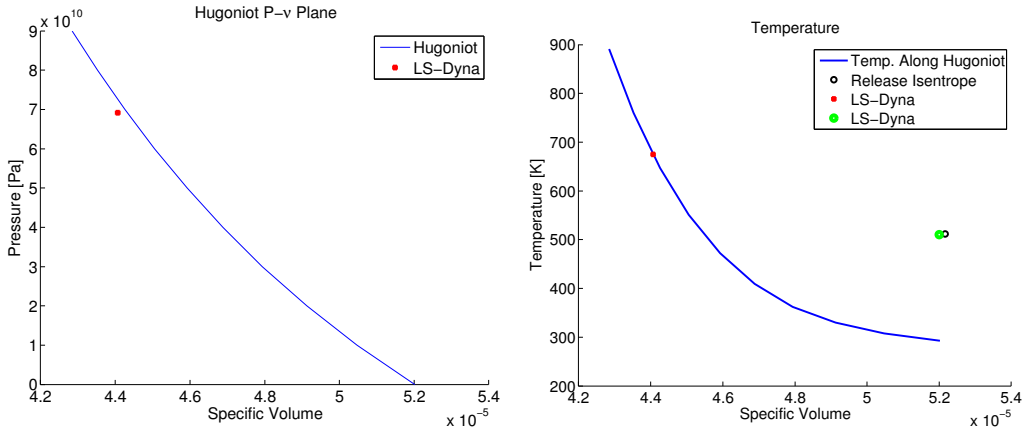


(a) (b)

**Figure 3.3**: (a) The final calculated states on the P$-\nu$ plane agree with Hugoniot data obtained from (Kinslow, 1970) (b) Final temperature of the simulation on both loading (red dot) and unloading process (green dot) match up data from (Kinslow, 1970) for pure Tungsten.

evolution of the temperature along the Hugoniot of the material and also temperature after unloading.

These results for the homogeneous materials give us a confidence that LS-DYNA calculations will correctly capture the dissipative processes of the laminated composite where multiple shock loading and unloading take place driving the material to the steady state.

Another important issue is the rise time of shock waves in each material which is an important space scale for the modeling of laminate composites. Of course it is desirable that the shock width is similar to experimental values, but it is not important for the parameters of the final state as long as the shock width is smaller than the layer thickness ensuring that the material will reach Hugoniot states at each shock loading. These Hugoniot states are characteristic for stationary shocks and are independent of the specific mechanisms of dissipation and resulting shock widths.

Calculations with a different value of viscosity and different mesh size were conducted to confirm that our approach gives the same values of temperatures.

The results of calculations for reduced viscosity and mesh size are presented in Fig. 3.4 (a)-(b) and 3.5 (a)-(b). From comparison of the results presented in Figs. 3.2 and 3.3 (a)-(b) and in Figs. 3.4 and 3.5 (a)-(b) we may conclude that final states do not depend on artificial viscosity and mesh size.

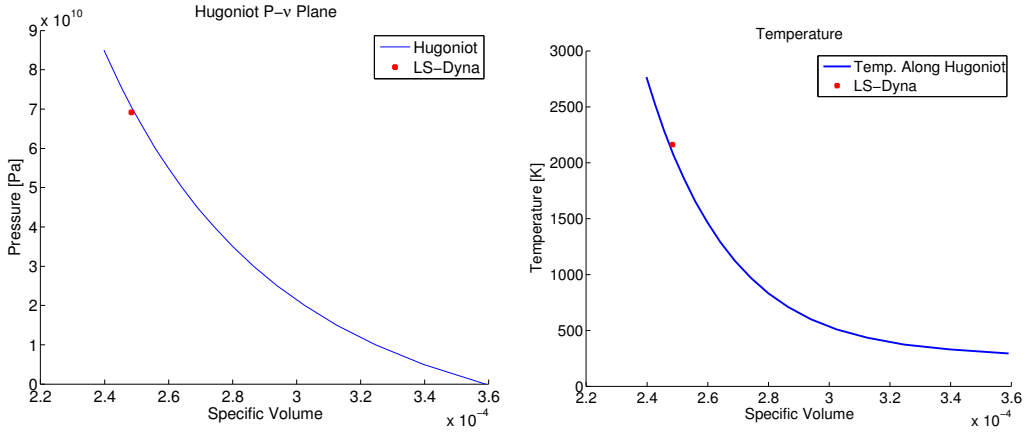


(a) (b)

**Figure 3.4**: (a) Final state on the P$-\nu$ plane for calculations with small shock viscosity and refined mesh (b) Final temperature for calculations with small shock viscosity and refined mesh.

Recent experimental data for shock rise time in Al at the range of 2 to 45 GPa demonstrated good correlation with Swegle-Grady equation (Crowhurst et al., 2011). Using data from (Crowhurst et al., 2011) for Al at 43 GPa we get a shock width equal to .18 micron and a shock wave rise time $\Delta$t=20x10$^{-12}$ s. In Fig. 3.6 the profile of particle velocity shock wave calculated in a pure Al bar at pressure 43 GPa is presented. We can see in Fig. 3.6(b) that artificial viscosity in our calculations using LS-Dyna resulted in the shock rise time equal $\Delta$t=3.1x10$^{-8}$ s or four orders of magnitudes larger than in experiments giving the shock width equal to 2.48x10$^{-4}$ m = 0.248 mm. In our calculations for shock waves in laminates we got maximum shock pressures at the vicinity of 70 GPa and final pressure of 43 GPa and shock widths at these pressure were equal to 2.52x10$^{-4}$ m = 0.252 mm and 2.48x10$^{-4}$ m = 0.248 mm correspondingly.

Using Swegle-Grady equation we get the following relation between shock

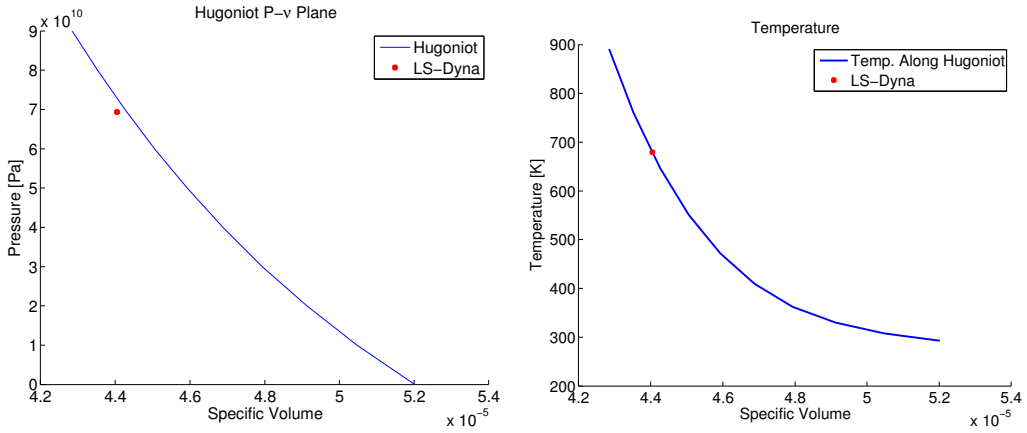


(a) (b)

**Figure 3.5**: (a) Final state on the P$-\nu$ plane for calculations with small shock viscosity and refined mesh (b) Final temperature for calculations with small shock viscosity and refined mesh.

rise time and particle velocity and stresses at two shocks:

$$\Delta t_2 = \left(\frac{\sigma_1}{\sigma_2}\right)^5 \left(\frac{u_2}{u_1}\right)^2 \Delta t_1 \tag{3.1}$$

Using available data for shock width for Al at 43 GPa and the equation above we get the following shock width for Al at 70 GPa of 0.16x10$^{-6}$ m = 0.00016 mm with a rise time $\Delta$t=5.8x10$^{-12}$ s. We can see that at 70 GPa we also have a large difference between rise times in our LS-Dyna calculations and in experiments. But it is important that shock width in our calculations was smaller than the thickness of the thin layers ensuring steady shock wave propagation in each Al and W layer and corresponding Hugoniot states after single shock loading.

(Asay et al., 1980) compiled results on shock rise time for tungsten at different stress levels up to a shock pressure close to 10 GPa. A shock rise time in the paper (Asay et al., 1980) is equal to 2.75x10$^{-7}$ s corresponding to a stress level of 9.92 GPa. At similar shock pressure in our LS-Dyna calculations at a stress level of 9.9 GPa we obtain a result of $\Delta$t=3.05x10$^{-7}$ s. Using equation 3.1 above and value of $\Delta$t = 2.75x10$^{-7}$ s for a shock wave at pressure 9.9 GPa we obtain for W at a pressure of 70 GPa a shock rise time equal to $\Delta$t=6.82x10$^{-10}$ s and shock width

equal to 3x10$^{-6}$ m while at 43 GPa we obtain a rise time equal to $\Delta$t=3.4x10$^{-9}$ s and shock width equal to 1.6x10$^{-5}$ m. Our LS-Dyna calculations give a rise time for 43 GPa and 70 GPa of $\Delta$t=6.3x10$^{-8}$ s and $\Delta$t=4.6x10$^{-8}$ s, respectively, with their corresponding shock width of 0.292x10$^{-3}$ m and 0.23x10$^{-3}$ m.

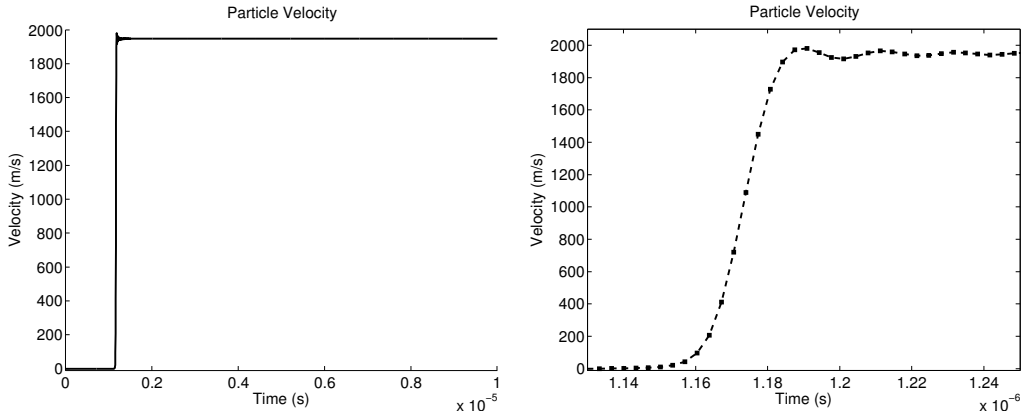


(a) (b)

**Figure 3.6**: (a) Particle Velocity in Aluminum from LS-Dyna calculations at a stress level of 43 GPa (b) Particle Velocity in Aluminum from LS-Dyna calculations at a stress level of 43 GPa.

The shock width in LS-DYNA calculations is smaller but comparable to the smallest size of Al layers (0.5 mm) still being smaller than largest size of Al layer equal 2 mm, the similar situation is with W layers.

The challenge in calculating the shock loading of laminates at high shock pressures is related to large disparity of shock width, cell sizes and distances for reaching a final state behind shock and multiple shock loading-unloading cycles bringing the material to a final equilibrium state. We used different size of cells (from 1 mm to 4 mm) to prove whether different thermodynamic states will be reached behind shock waves in laminates because the number of shock reverberations before final state is reached may depend on the cell size at similar conditions of loading especially for a relatively short loading pulses. We plan to do calculations with a smaller artificial viscosity and mesh sizes providing shock width significantly smaller than size of layers in laminate.

In Fig. 3.8 LS-DYNA results with an improved rise time are presented for

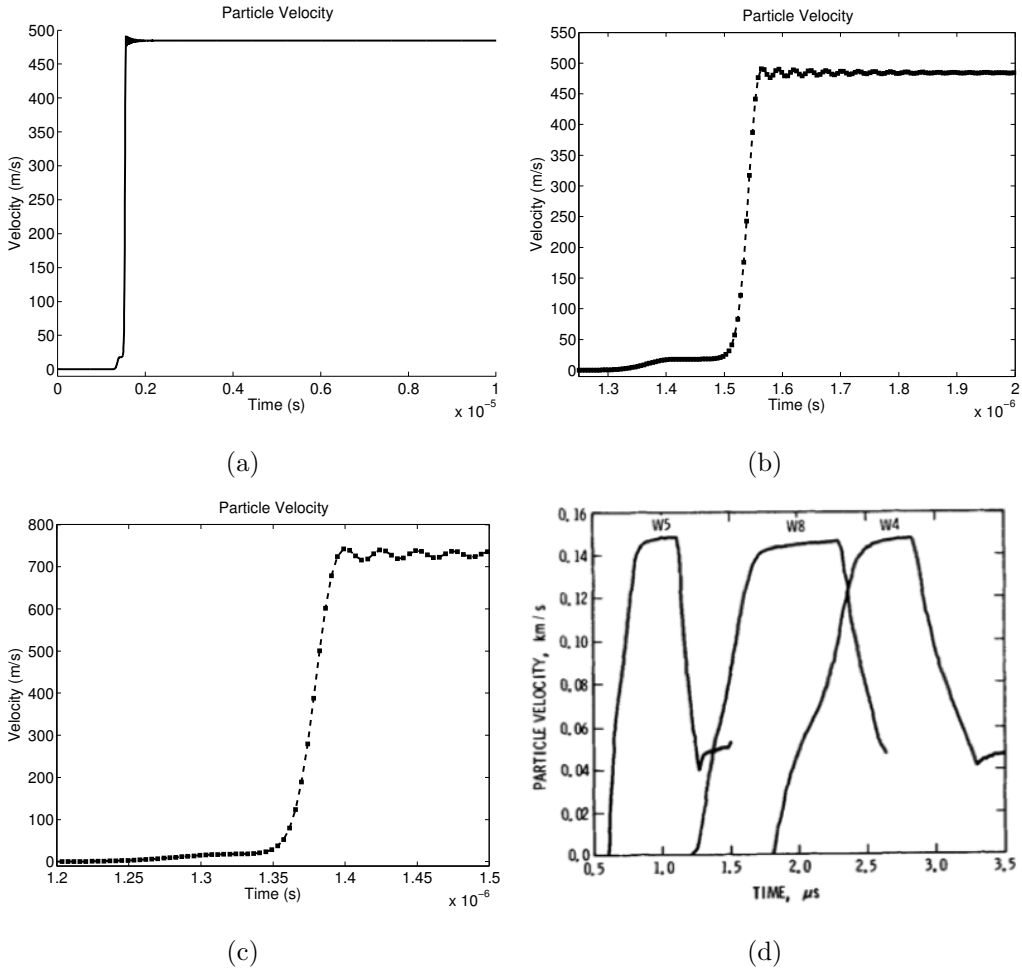


**Figure 3.7**: (a) Particle Velocity from in Tungsten from LS-DYNA calculations at a stress level of 43 GPa (b) Particle Velocity in Tungsten from LS-DYNA calculations at a stress level of 43 GPa. (c) Rise of Particle Velocity at 70 Gpa (d) Particle velocity reprint from (Asay et al., 1980) at 9.9, 9.53 and 9.63 GPa. Figure 3.7 (b) and 3.7 (c) represent calculations with a low shock viscosity and refined mesh to achieve a shock width that is around 10 times smaller than the .5mm layer.

both Al and W at 70 GPa shock pressure. Under these conditions, the width for the plastic wave on the Aluminum bar is $4.5653 \times 10^{-8}$ m = .0457 mm with a rise time $\Delta t = 4.94 \times 10^{-9}$ s. This implies that the width of the wave is about 11 times smaller than thickness of the smallest Al layer in the laminate. For W the width of

the wave is of 3.9815x10$^{-5}$ m = .0398mm with a shock rise time $\Delta$t=8.0480x10$^{-9}$ s, thus the width of the shock is about 12 times smaller than the smallest W layer in the laminate. It is also important that mesh size ensures that there are about 4 elements in a shock width in W and about 5 elements in shock width in Al.

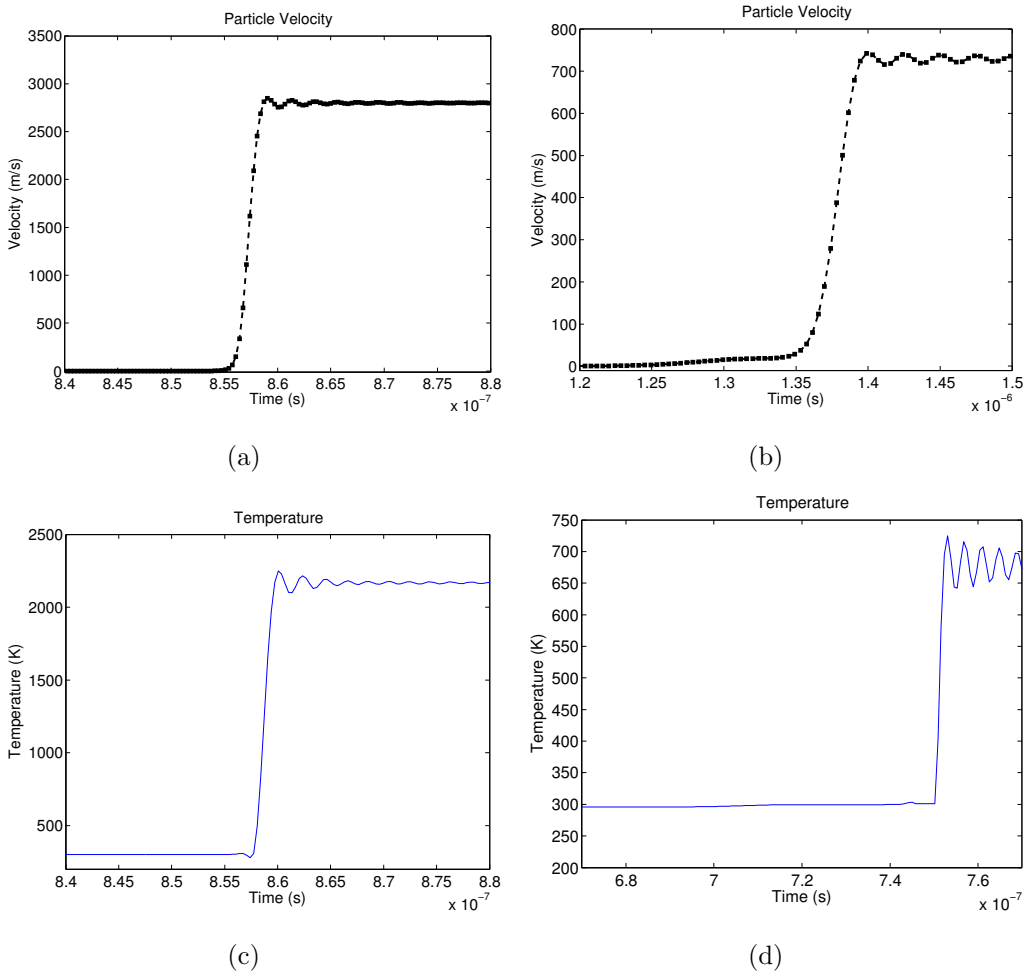


**Figure 3.8**: (a) Particle Velocity in Aluminum from LS-DYNA calculations at a stress level of 70 GPa (b) Particle Velocity in Tungsten from LS-DYNA calculations at a stress level of 70 GPa. (c) Temperature calculated on Aluminum loaded at 70 GPa (d) Temperature calculated on Tugnsten loaded at 70 GPa. These calculations were done with a low shock viscosity and a refined mesh to achieve a width of the wave that is around 10 times small than the .5mm layer.

Chapter 3, partially, is to be used in a subsequent publication. The thesis author is going to be the primary investigator and author of this paper.

# Chapter 4

# Theoretical Models

Two main approaches called the Average Isotherm and Average Kinematic Model were analyzed in this study. These models were selected for their simple implementation and the agreement with experimental data mentioned by (Petel and Jetté, 2009). Aside from the comparisons of the laminate Hugoniot based on these models, a thermo-dynamical approach to determine the temperature along the Hugoniot originally proposed by (McQueen et al., 1967) was also explored.

## 4.1 Average Isotherm Method

Presented by (McQueen et al., 1967) and reviewed by (Petel and Jetté, 2009) this model approaches the problem from a thermodynamic point of view and allows calculation of the individual isotherms using the individual Hugoniot by means of Eqn.4.1.

$$\Big(\frac{dP}{dv}\Big)_{0K} - \frac{\Gamma_0}{v_0}P_{0K} = \frac{\Gamma_0}{2v_0}\Big[P_H + \Big(\frac{2v_0}{\Gamma_0} + v - v_0\Big)\Big(\frac{dP}{dv}\Big)_H\Big], \tag{4.1}$$

where indices $0K$ accounts for the $0K$-isotherm, $H$ for the parameter on Hugoniot, $v$ refers to the specific volume of the material, $\Gamma$ is the Grüneisens Gamma and $P_H$ in the Eqn.4.1 is given by

$$P_H = \frac{C_{0i}^2(v_{0i} - v_i)}{[v_{0i} - S_i(v_{0i} - v_i)]^2}, \tag{4.2}$$

where $C_{0i}$ and $S_i$ are parameters used for the linear fit of the Hugoniot on the $U$-$u$ plane, the actual values used in this paper can be found in Table 3.1. An important remark to this approach is that the Hugoniot states are treated as a thermodynamically equilibrium states.

Since the main interest of this paper is related to the behavior of mixtures, the following mixture rules are introduced (Petel and Jetté, 2009):

$$v = X_a v_a + (1 - X_a) v_b, \tag{4.3a}$$

$$\frac{v_0}{\Gamma_0} = X_a \frac{v_{0a}}{\Gamma_{0a}} + (1 - X_a) \frac{v_{0b}}{\Gamma_{0b}}. \tag{4.3b}$$

where $X_a$ is the mass fraction of component a of the mixture. Once the individual isotherms of each component of the mixture are calculated it is possible to establish the mixture isotherm and use Eqn.4.1 to solve for the Hugoniot. The results from this calculation lie on the $P$-$v$ plane.

It should be mentioned that in (Petel and Jetté, 2009) no attempt to calculate temperatures in mixtures focusing only on specific volume and pressure.

## 4.2 Kinetic Energy Average Method

(Batsanov, 1994) originally postulated that a mixture that has already reached pressure equilibrium, an equilibrium material velocity can also be determined by averaging the material velocities on the individual Hugoniots using the following mixture rule

$$u_{mix}^2 = X_a u_a^2 + (1 - X_a) u_b^2, \tag{4.4}$$

where $u_a$ and $u_b$ are the particle velocities behind shock waves in corresponding materials defined by

$$u_i = \frac{C_{0i}}{2S_i} \left( \sqrt{1 + \frac{4 S_i v_{0i} P}{C_{0i}^2}} - 1 \right), \tag{4.5}$$

The results of this method lie in the $P$-$u$ plane. In order to make meaningful comparisons between the two approaches and the simulation results, all results

must be represented in the same plane, in this case the $P$-$v$ plane. This change is easily achieved through the classical conservation equations, known as the Euler equations in one dimension

$$\frac{\partial \rho}{\partial t} + \frac{\partial \rho u}{\partial x} = 0, \tag{4.6a}$$

$$\frac{\partial \rho u}{\partial t} + \frac{\partial (\rho u^2 + P)}{\partial x} = 0, \tag{4.6b}$$

$$\frac{\partial \rho e}{\partial t} + \frac{\partial u(\rho e + \rho \frac{u^2}{2} + P)}{\partial x} = 0, \tag{4.6c}$$

where $P$ is the pressure of the material, $e$ is the internal energy and $u$ the particle velocity. These equations can be written for a stationary wave as following:

$$\rho_0 U = \rho(U - u), \tag{4.7a}$$

$$P - P_0 = \rho_0 U u, \tag{4.7b}$$

$$\Big[(E - E_0) - \frac{u^2}{2}\Big]\rho_0 U = P_0 u, \tag{4.7c}$$

where $U$ is the steady shock wave velocity. Combining Equations 4.7a and 4.7b explicit expressions for $U$ and $u$ in terms of $P$ and $v$ and can be derived as follows:

$$\frac{P - P_0}{\rho_0 U} = u, \tag{4.8}$$

we now plug-in this expression of $u$ into 4.7a to find $U$ which leads to the following equation

$$\rho_0^2 U_s^2 = \frac{\rho(P - P_0)}{\frac{\rho}{\rho_0} - 1} = \frac{P - P_0}{\frac{1}{\rho_0} - \frac{1}{\rho}} = \frac{P - P_0}{v_0 - v}, \tag{4.9}$$

and finally yields

$$U = v_0 \sqrt{\frac{P - P_0}{v_0 - v}}, \tag{4.10}$$

where $v$ corresponds to the specific volume $(\frac{1}{\rho})$. Following an analogous procedure an explicit expression in terms of only pressure and specific volume can also be found for u:

$$u = \sqrt{(P - P_0)(v_0 - v)}, \tag{4.11}$$

finally by using the Eqns 4.10 and 4.11 and 4.7cit is possible to write the change in energy in terms of pressure and specific volume as follows

$$E - E_0 = \frac{(P + P_0)(v_0 - v)}{2}. \tag{4.12}$$

It should be mentioned that these equations are not sensitive to particular mechanism of dissipation or to the shock width/shock rise time.

## 4.3 Final Temperature Calculation

To find the temperature of the material along its Hugoniot we will follow the approach originally proposed by (McQueen et al., 1967). First, we introduce the thermodynamic law

$$dE = TdS - Pd\nu, \tag{4.13}$$

which is accompanied by the following thermodynamic identity, this identity comes from manipulation of the first thermodynamic law (4.13) by rewriting $dE = C_v dT$ and knowing that $\Gamma = \frac{V}{C_v}(\frac{P}{T})$

$$TdS = C_\nu dT + C_\nu T\Big(\frac{\Gamma}{\nu}\Big)d\nu, \tag{4.14}$$

In order to get an equation that explicitly gives the temperature in terms of the shock pressure and specific volume, we take Eqn. 4.7c and differentiate it in terms of $P$ and $v$ with the following result

$$dE = \frac{(\nu_0 - \nu)}{2}dP - \frac{(P + P_0)}{2}d\nu, \tag{4.15}$$

Using Eqn. 4.15 and plugging into Eqn. 4.13 the following expression is found

$$TdS = \frac{(\nu_0 - \nu)}{2} dP + \frac{(P - P_0)}{2} d\nu, \tag{4.16}$$

Finally, Eqn. 4.16 can be combined with Eqn. 4.14 to yield the final expression that gives out directly the temperature

$$dT = \frac{\nu_0 - \nu}{2} dP + \left[ \frac{P - P_0}{2C_\nu} - T\left(\frac{\Gamma}{\nu}\right) \right] d\nu, \tag{4.17}$$

Through all the calculations, it is important to update $\Gamma$ (failing to do so would imply an infinite compressibility)

$$\Gamma\rho = \Gamma_0\rho_0, \tag{4.18}$$

In the same fashion, as the loading process take place, there is a need to update $C_v$ , for this case a simple form of the Debye theory was selected, this theory offers an adequate representation of the specific heat. (Kinslow, 1970) propose the use of only one Debye Temperature $\Theta(V)$ which is only a function of the volume. It is possible now to determine the $C_v$ of the material by means of the following expression:

$$C_\nu = 3nk \left[ 4D_3(x) - \frac{3x}{e^x - 1} \right], \tag{4.19}$$

where k is the Boltzmanns constant, n is the number of atoms per gram and $D_3$(x) can be found using the following expression,

$$D_3(x) = \frac{3}{x^3} \int_0^x \frac{z^3}{e^z - 1} dz, \; x = \frac{\Theta}{T}, \tag{4.20}$$

It is important to notice that this is consistent with the assumption that the Grüneisen parameter only depends on the volume.

Now, to determine the temperature along the Hugoniot of the mixture we use the temeratures calculated along the Hugoniot Curve for each material (Al and W) and average them using 4.21

$$T = \frac{m_{Al} C_{P,Al} T_{Al} + m_W C_{P,W} T_W}{m_{Al} C_{P,Al} + m_W C_{P,W}}. \tag{4.21}$$

This equation takes into account the different heat capacity of Al and W and weights the contribution to the final temperature using the mass of each element.

Chapter 4, partially, is to be used in a subsequent publication. The thesis author is going to be the primary investigator and author of this paper.

# Chapter 5

# Results on Al/W Layered Composite

## 5.1 Shock evolution under the loading by a 80mm impactor in different cell size Al-W layered composite.

### 5.1.1 Al-W laminate with 4mm Cells (2mm Layers)

In Fig. 5.1 the evolution of shock wave with the depth in laminate with cell size 4 mm is presented. From this figure we can conclude that for a relatively short time of loading pulse, determined by the thickness of the Al impactor (80 mm), the shock wave did not reach a steady state. For example, we see oscillations of pressure behind the shock which did not attenuate before arrival of release wave from the free surface of impactor. Thus nonsteady behavior of shock wave is observed even for a laminate material at depths up to 220 mm which is much larger than cell size. Before reaching a steady state a rarefaction wave is catching with the oscillatory part of the shock. At the same time it is interesting that the leading part of the oscillatory shock wave and the amplitude of the leading pulse and its rise time reached a steady value demonstrated by Fig. 5.2 and Fig. 5.3. We will see later in Chapter 6 that the leading part is really close to the steady

state of stationary wave in laminate under loading by long pulse.

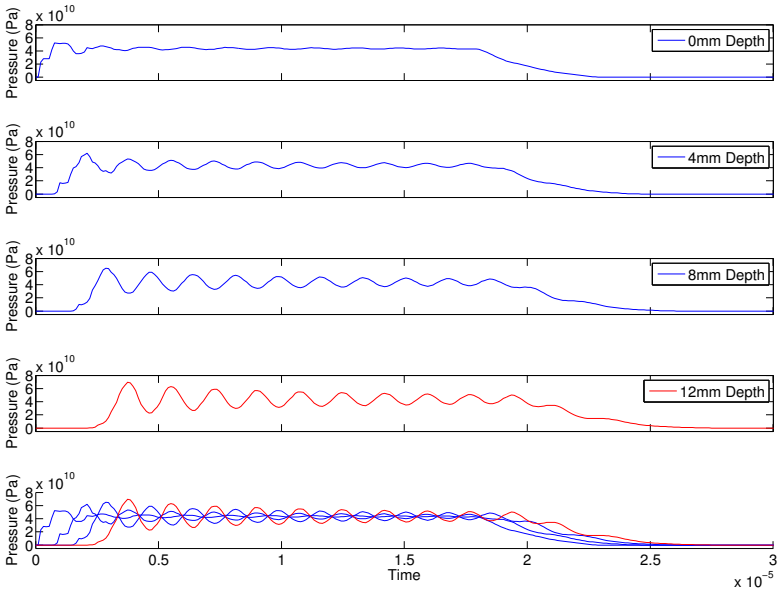


(a)

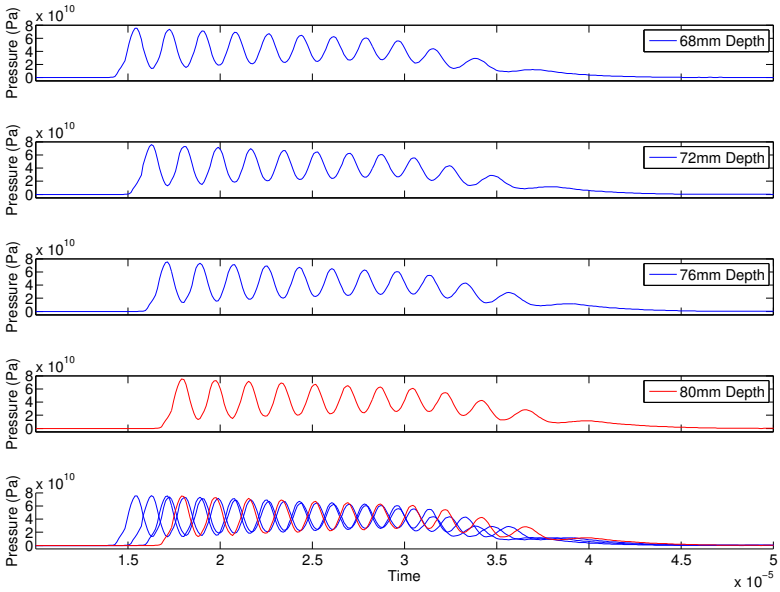


(b)

**Figure 5.1**: (a)-(d) Pressure Evolution vs. Time at different depths with 80 mm impactor and 2mm layers (4mm cells).

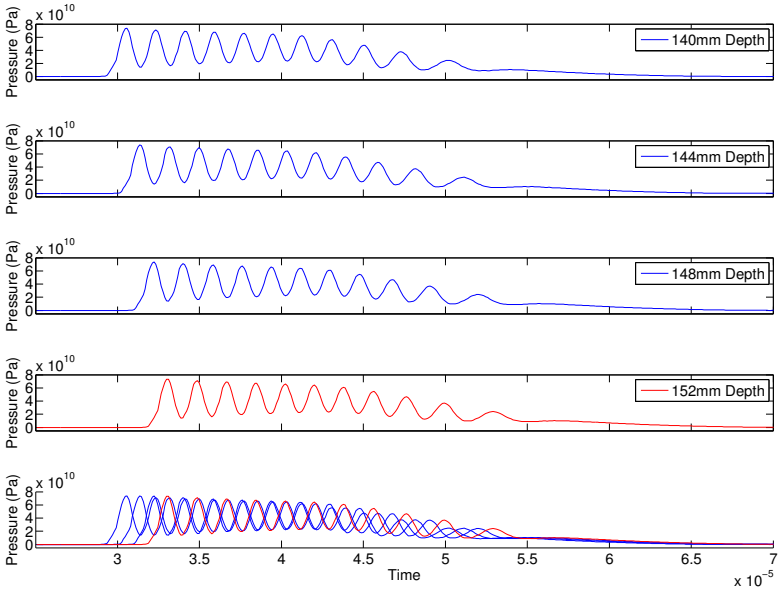


(c)

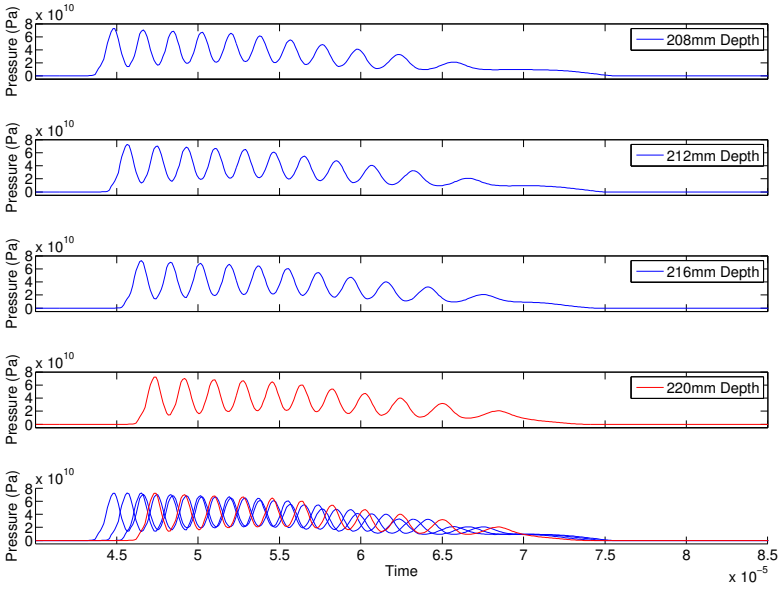


(d)

**Figure 5.1:** continued

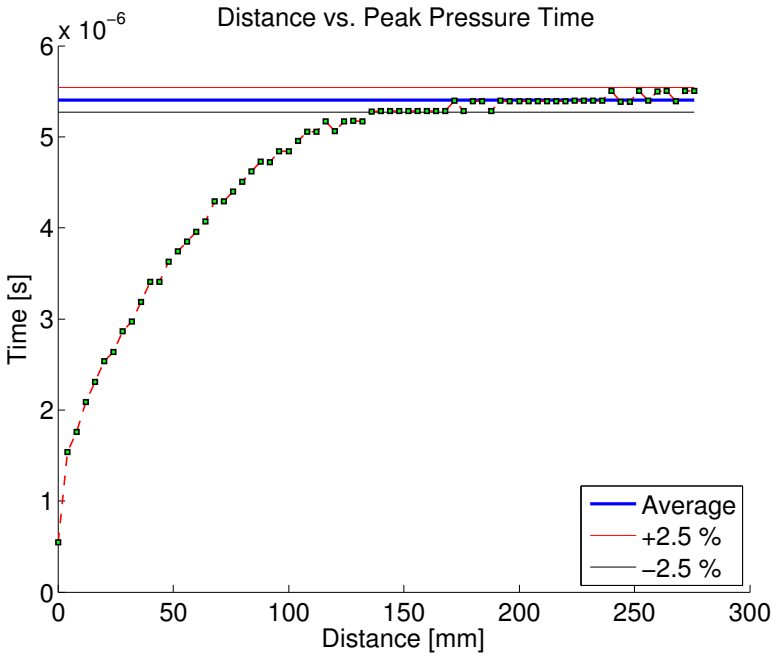


**Figure 5.2**: Distance vs. Time to maximum amplitude on a 4mm cells Al-W layered composite.

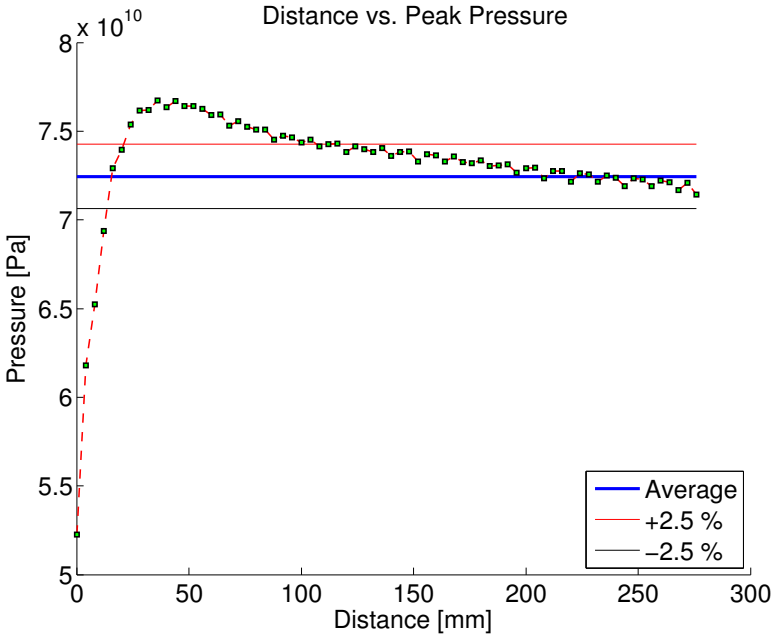


**Figure 5.3**: Distance vs. Maximum Pressure on 4mm cells Al-W layered composite.

### 5.1.2 Al-W laminate with 2mm Cells (1mm Layers)

In Fig. 5.4 the evolution of shock wave with the depth in laminate with cell size 2 mm is presented. From this figure we can conclude that for a relatively short time of loading pulse, determined by the thickness of the Al impactor (80 mm), the shock wave did not reach a steady state. We see oscillations of pressure behind the shock which did not attenuate before arrival of release wave from the free surface of impactor. Thus nonsteady behavior of shock wave is observed even for a laminate material at depths up to 220 mm which is much larger than cell size. At the same time it is interesting that the leading part of the oscillatory shock wave and the amplitude of the leading pulse and its rise time reached in average a steady value demonstrated by Fig. 5.5 and Fig. 5.6. We will see later in Section 5.2.2 that the shock reaches a steady state when loaded by a long pulse.

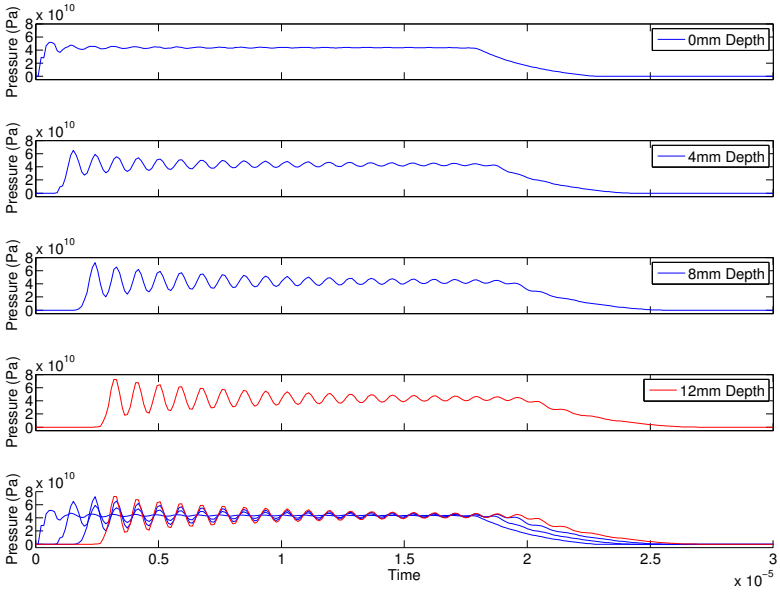


(a)

**Figure 5.4**: (a)-(d) Pressure Evolution vs. Time at different depths with 80 mm impactor and 1mm layers (2mm cells).

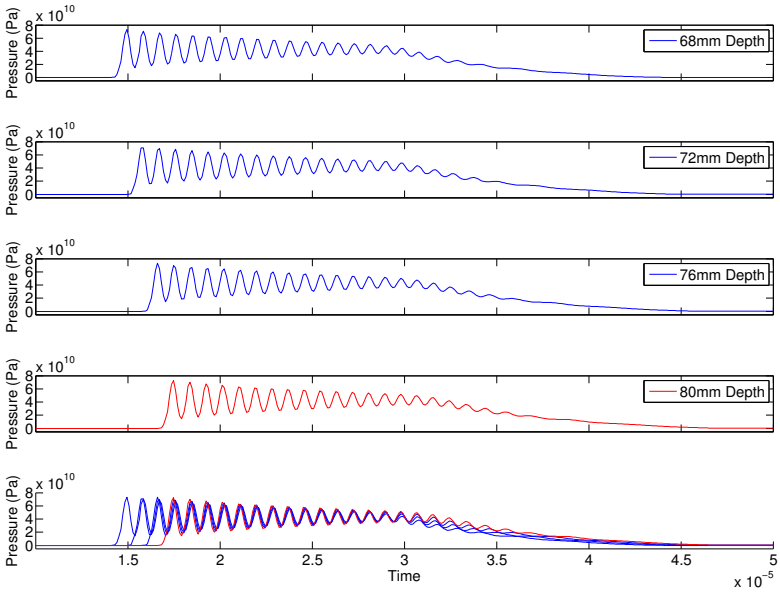


(b)

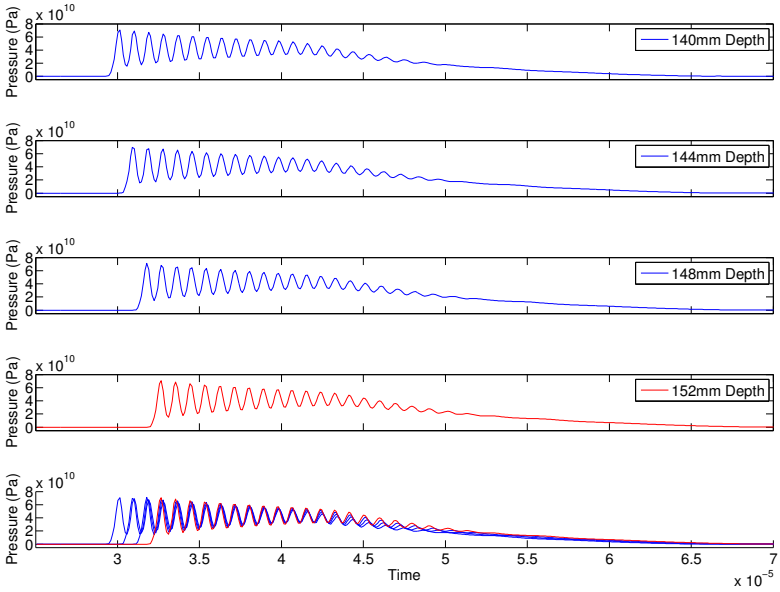


(c)

**Figure 5.4:** continued

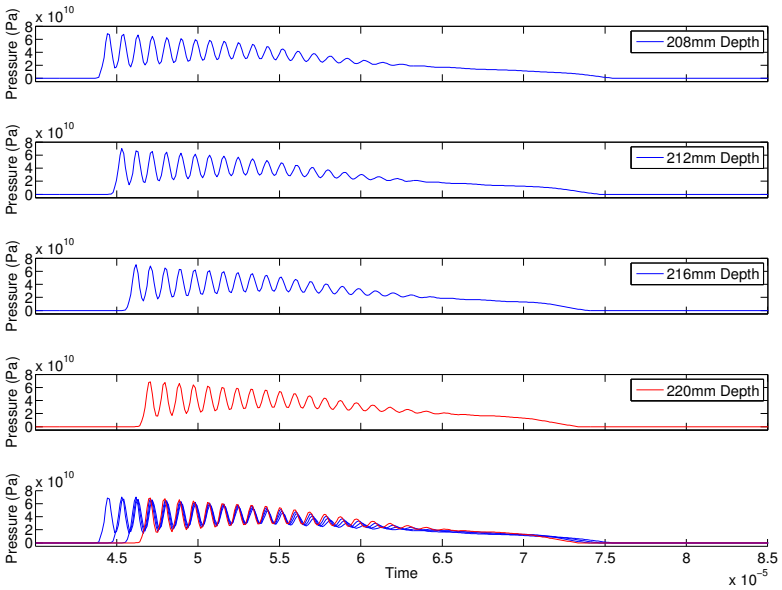


(d)

**Figure 5.4:** continued

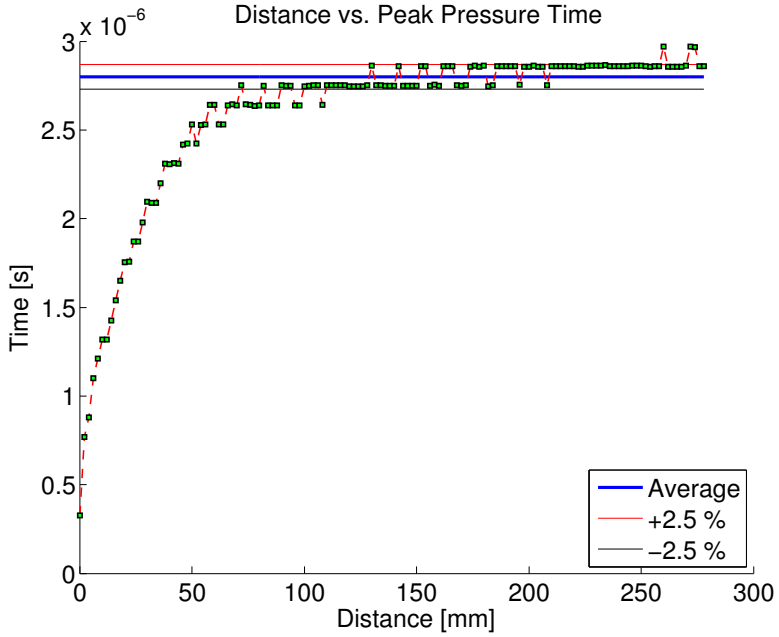


**Figure 5.5**: Distance vs. Time to maximum amplitude on a 2mm cells Al-W layered composite.

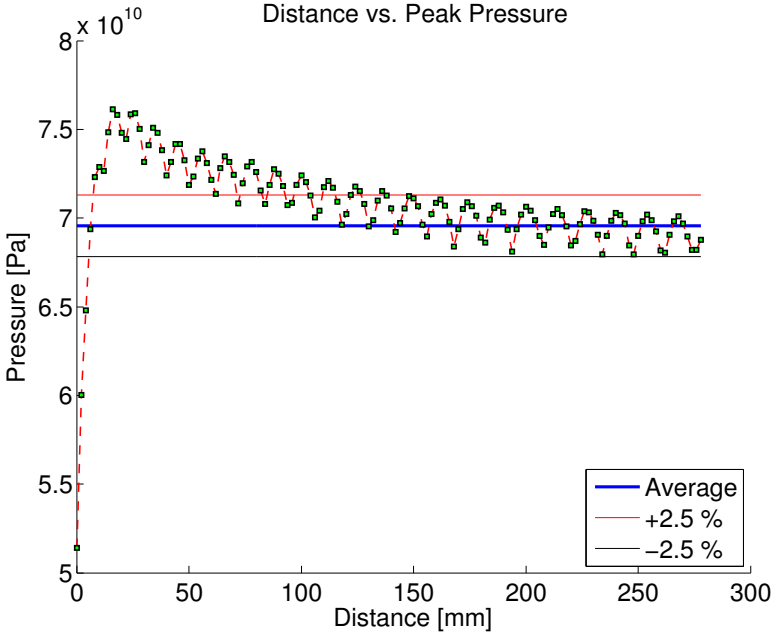


**Figure 5.6**: Distance vs. Maximum Pressure on 2mm cells Al-W layered composite.

### 5.1.3 Al-W laminate with 1mm Cells (0.5mm Layers)

In Fig. 5.7 the evolution of shock wave with the depth in laminate with cell size 1 mm is presented. From this figure we can conclude that for a relatively short time of loading pulse, determined by the thickness of the Al impactor (80 mm), the shock wave this time reached a steady state. We see that oscillations of pressure behind the shock attenuate and steady state is reached before arrival of release wave from the free surface of impactor. Oscillations behind shock quickly attenuate even at the very small depths from the impacted surface. It is interesting that the leading part of the oscillatory shock wave, the amplitude of the leading pulse and its rise time reached on average a steady values demonstrated by Fig. 5.8 and Fig. 5.9. But contrary to the other cases, there are strong oscillations around this average value which mechanism we plan to investigate in our future research.

It is important to mention that no steady state can be reached if linear elastic material model is used, in this case shock wave will be spread out without

reaching steady state.

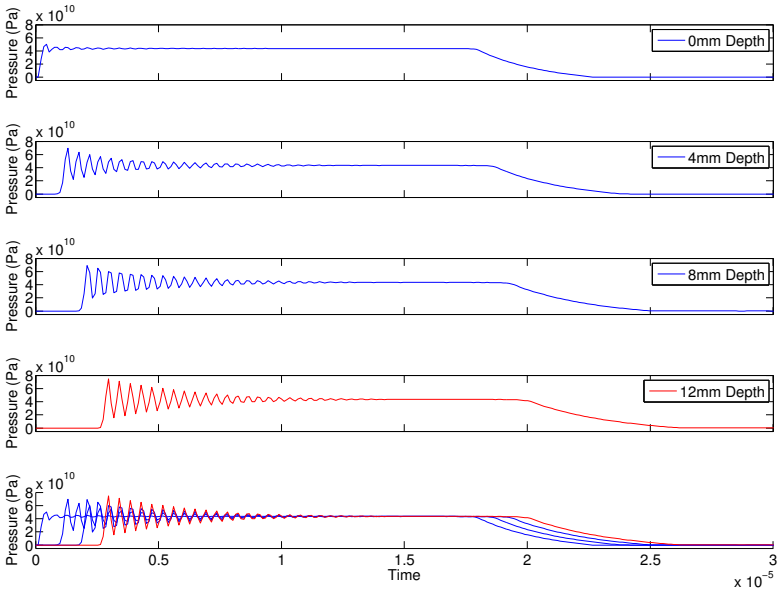


(a)

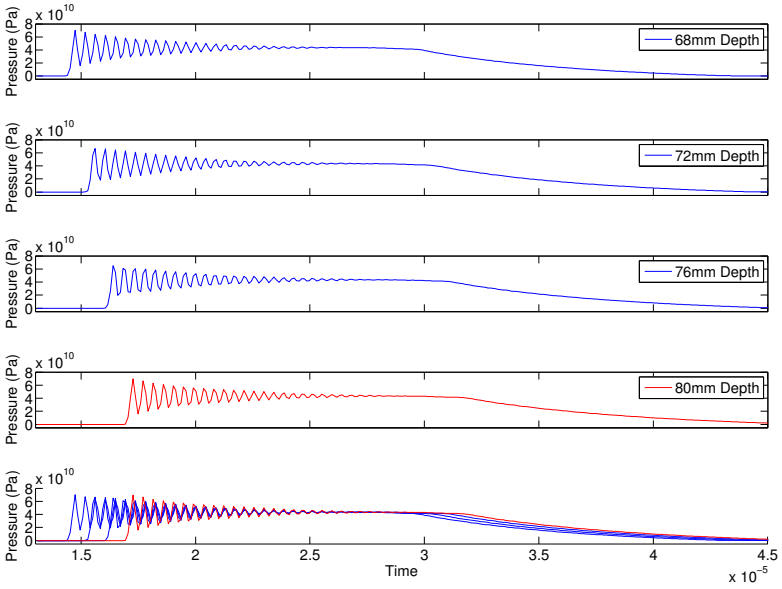


(b)

**Figure 5.7**: (a)-(d) Pressure Evolution vs. Time at different depths with 80 mm impactor and 0.5mm layers (1mm cells).

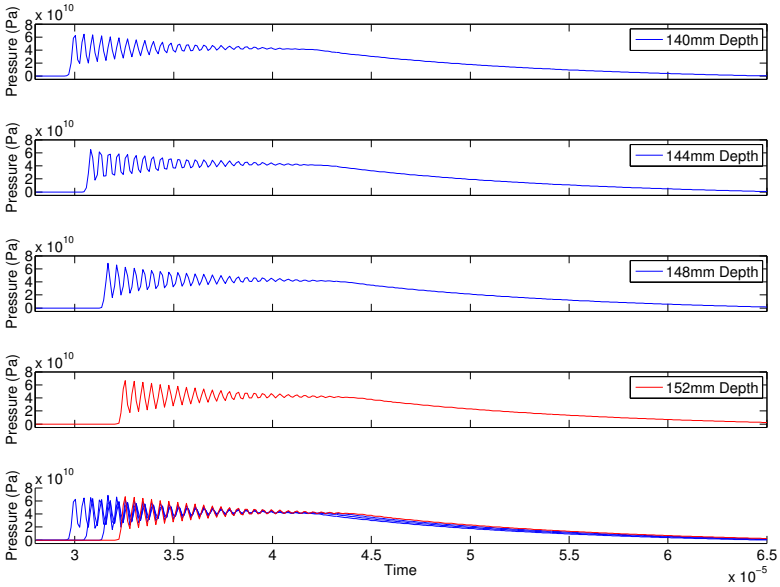


(c)

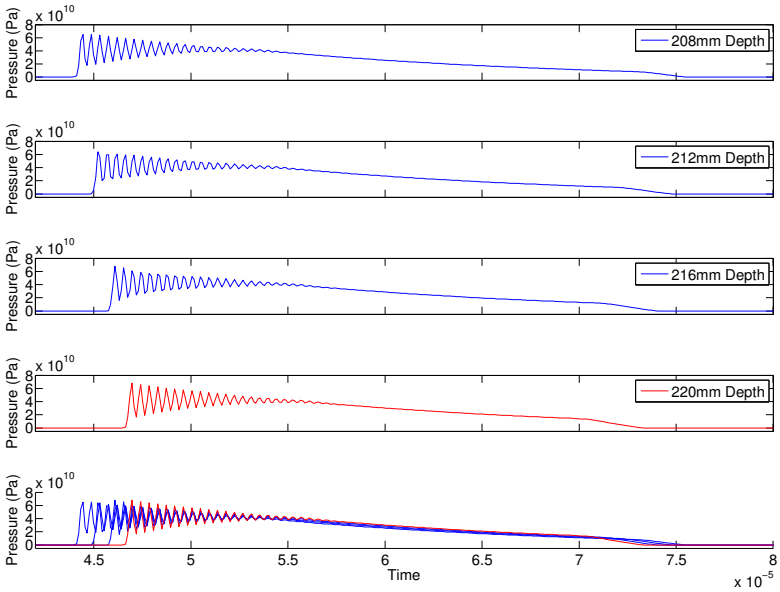


(d)

**Figure 5.7:** continued

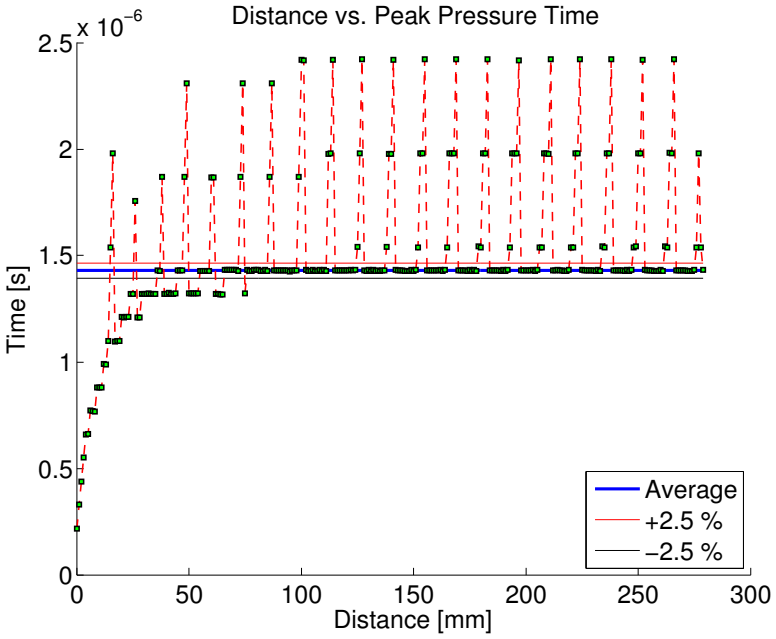


**Figure 5.8**: Distance vs. Time to maximum amplitude on a 1mm cells Al-W layered composite.

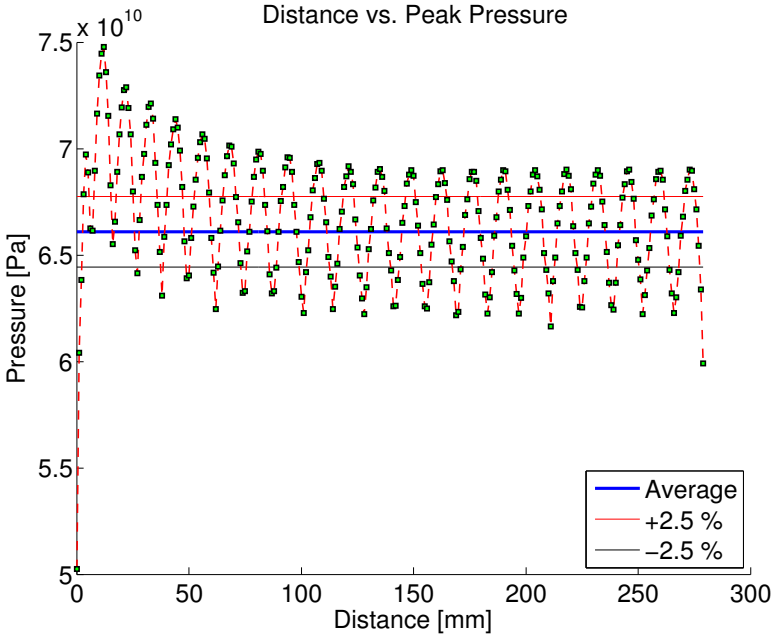


**Figure 5.9**: Distance vs. Maximum Pressure on 1mm cells Al-W layered composite.

## 5.2 Shock evolution under the loading by a 800mm impactor in different cell size Al-W layered composite.

### 5.2.1 Al-W laminate with 4mm Cells (2mm Layers)

In Fig. 5.10 the evolution of shock wave with the depth in laminate with cell size 4 mm is presented. From this figure we can conclude that for a relatively long time of loading pulse, determined by the thickness of the Al impactor (800 mm), the shock wave reaches a steady state, contrary to the short loading pulse already shown on section 5.1.1. For example, we see oscillations of pressure behind the shock which attenuate before arrival of release wave from the free surface of impactor. It is interesting that the leading part of the oscillatory shock wave and the amplitude of the leading pulse and its rise time reached a steady value demonstrated by Fig. 5.11 and Fig. 5.12. A real comparison with the sample loaded by the short pulse is presented on Chapter 6.

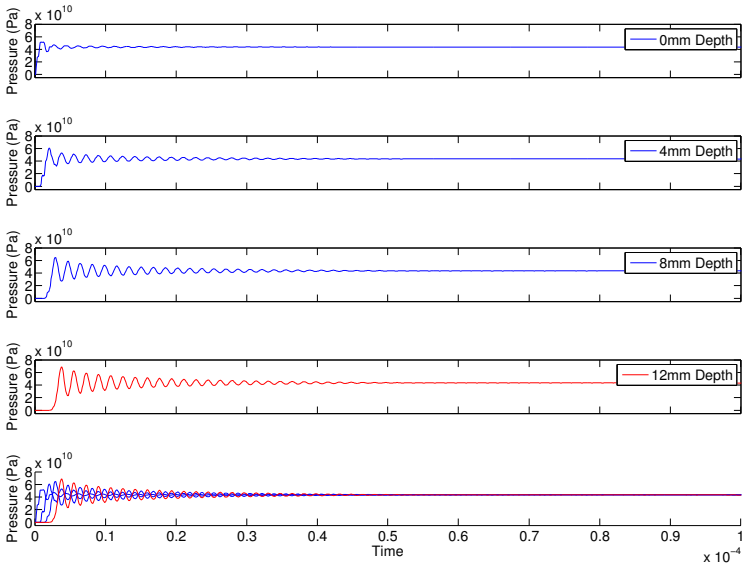


(a)

**Figure 5.10**: (a)-(d) Pressure Evolution vs. Time at different depths with 800 mm impactor and 2mm layers (4mm cells).

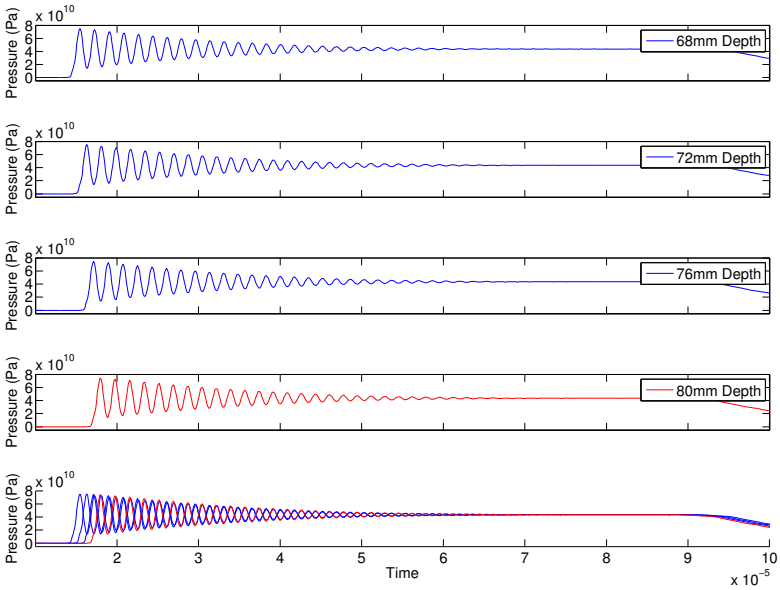


(b)

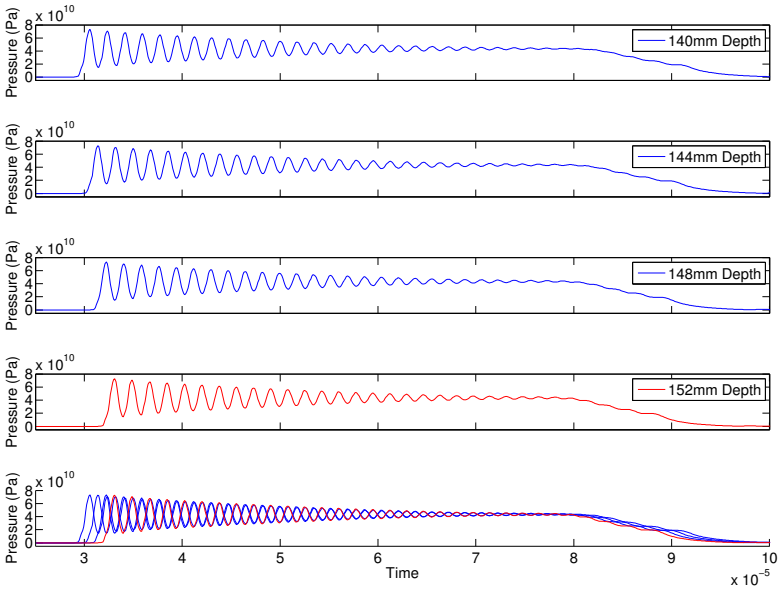


(c)

**Figure 5.10:** continued

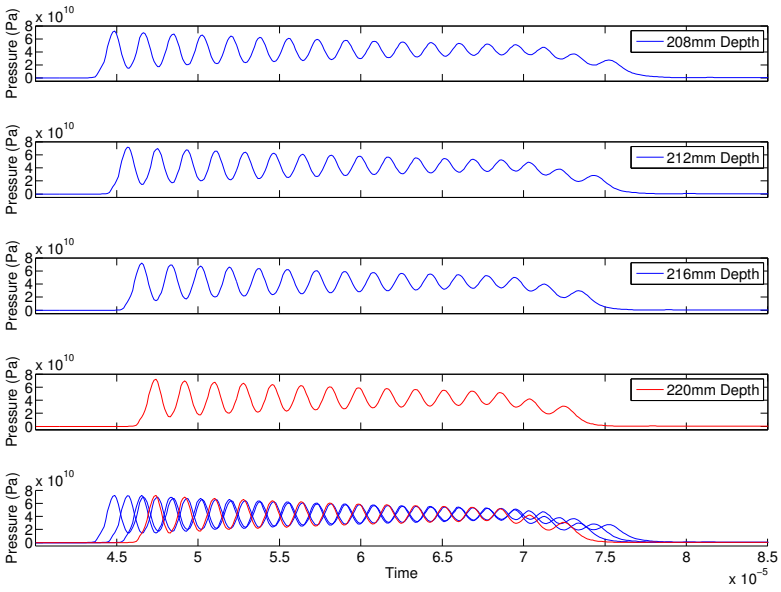


(d)

**Figure 5.10:** continued

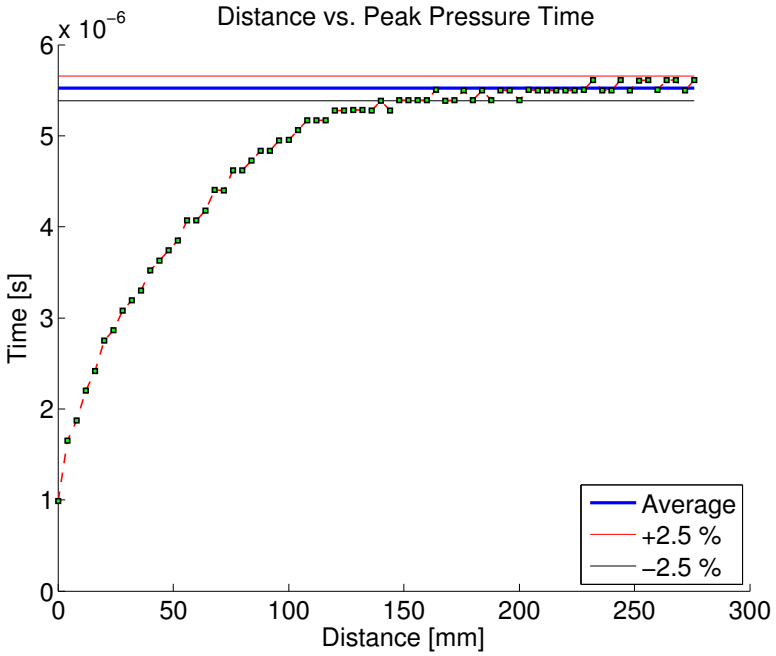


**Figure 5.11**: Distance vs. Time to maximum amplitude on a 4mm cells Al-W layered composite.

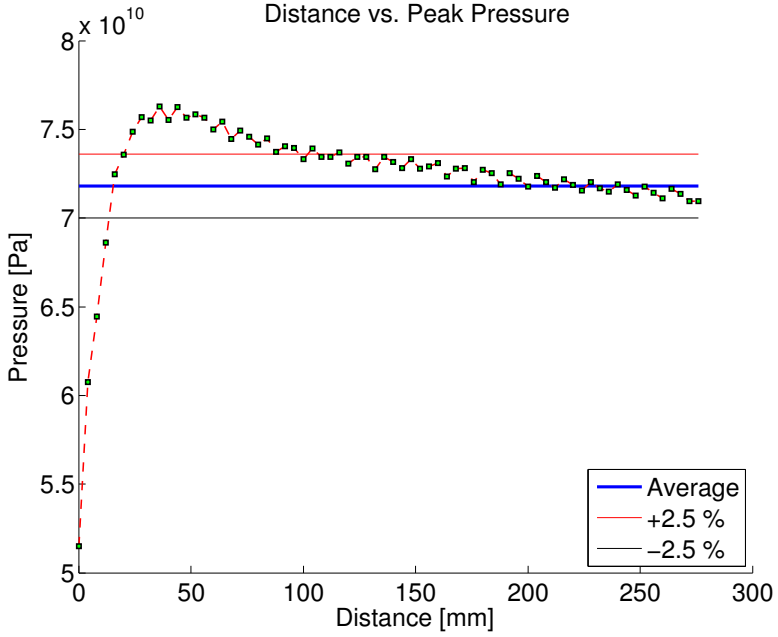


**Figure 5.12**: Distance vs. Maximum Pressure on 4mm cells Al-W layered composite.

### 5.2.2 Al-W laminate with 2mm Cells (1mm Layers)

In Fig. 5.13 the evolution of shock wave with the depth in laminate with cell size 2 mm is presented. From this figure we can conclude that for a relatively long time of loading pulse, determined by the thickness of the Al impactor (800 mm), the shock wave reaches a steady state, contrary to the short loading pulse already shown on section 5.1.2. We see oscillations of pressure behind the shock which attenuate before arrival of release wave from the free surface of impactor. It is interesting that the leading part of the oscillatory shock wave and the amplitude of the leading pulse and its rise time reached a steady value demonstrated by Fig. 5.14 and Fig. 5.15. A comparison with the sample loaded by the short pulse is presented on Chapter 6.

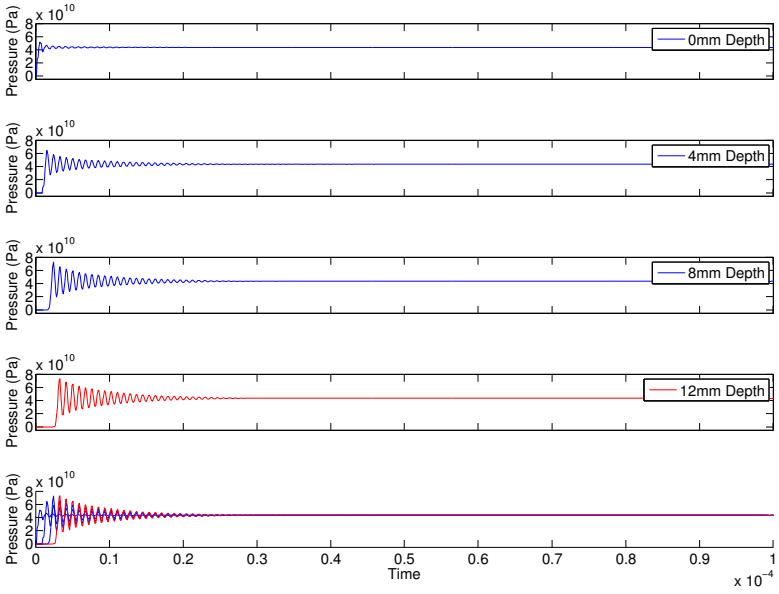


(a)

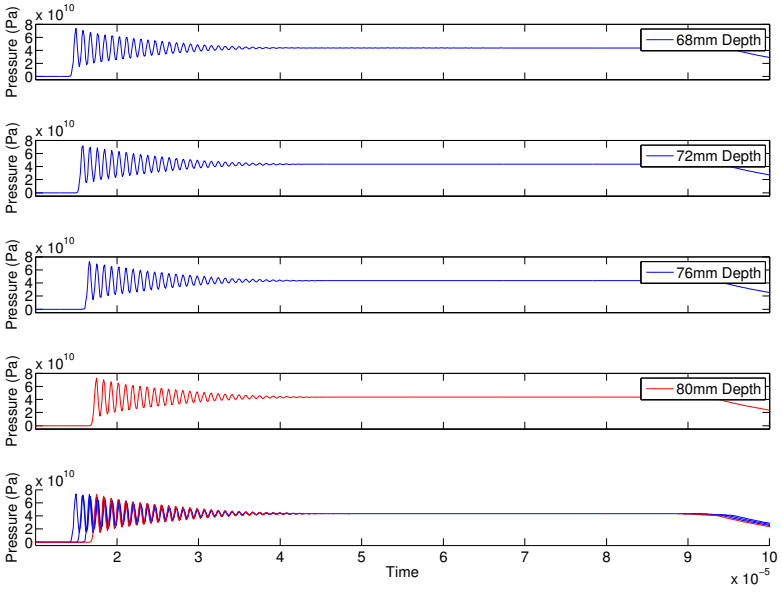


(b)

**Figure 5.13**: (a)-(d) Pressure Evolution vs. Time at different depths with 800 mm impactor and 1mm layers (2mm cells).

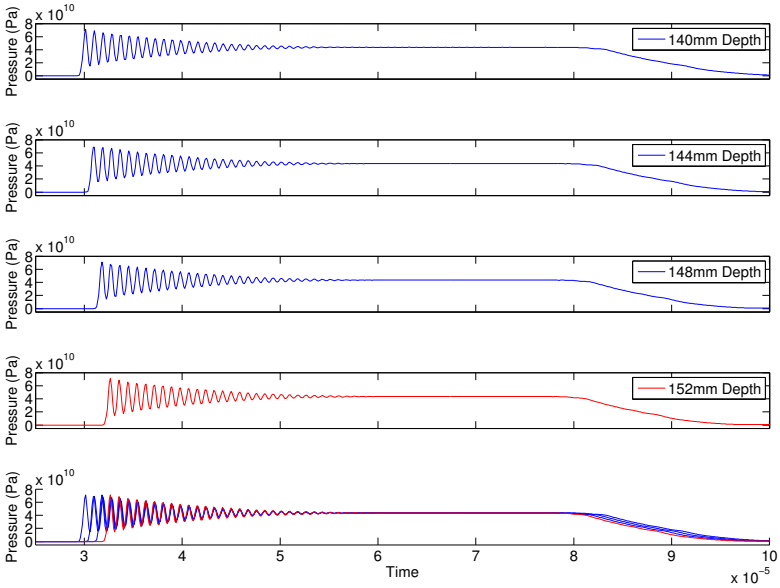


(c)

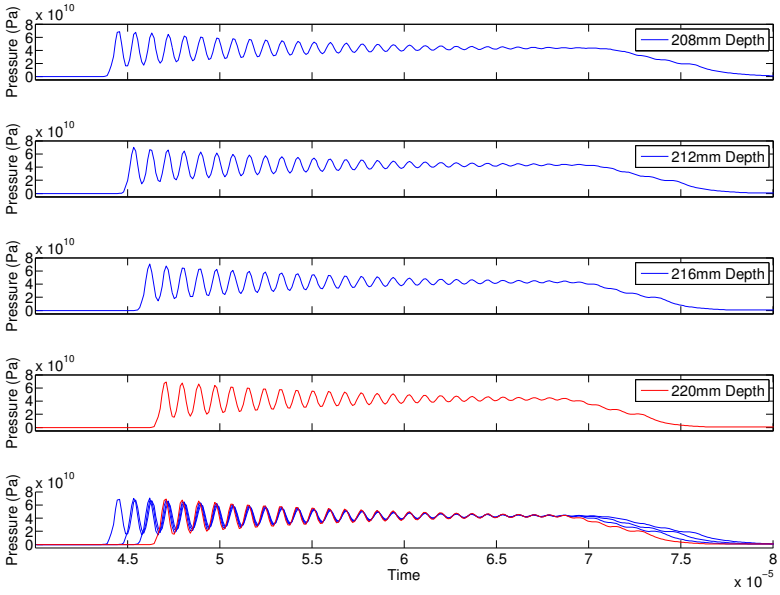


(d)

**Figure 5.13:** continued

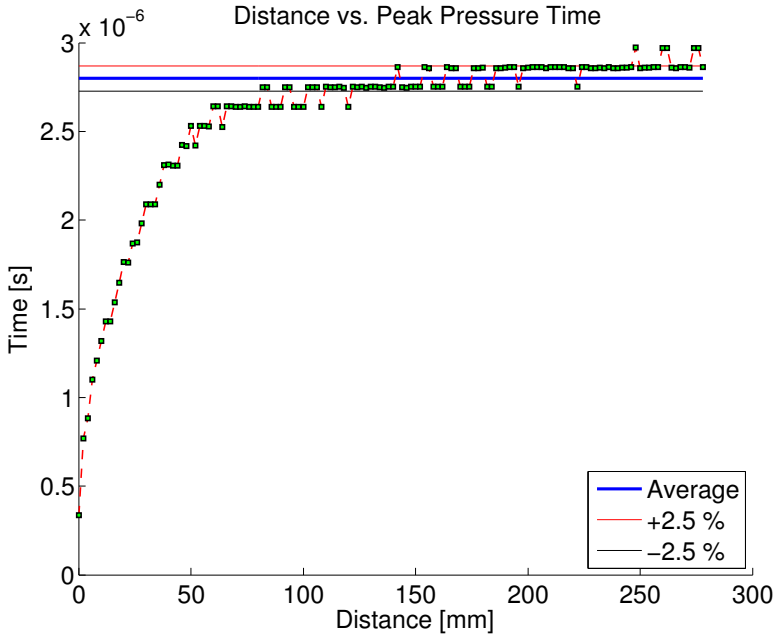


**Figure 5.14**: Distance vs. Time to maximum amplitude on a 2mm cells Al-W layered composite.

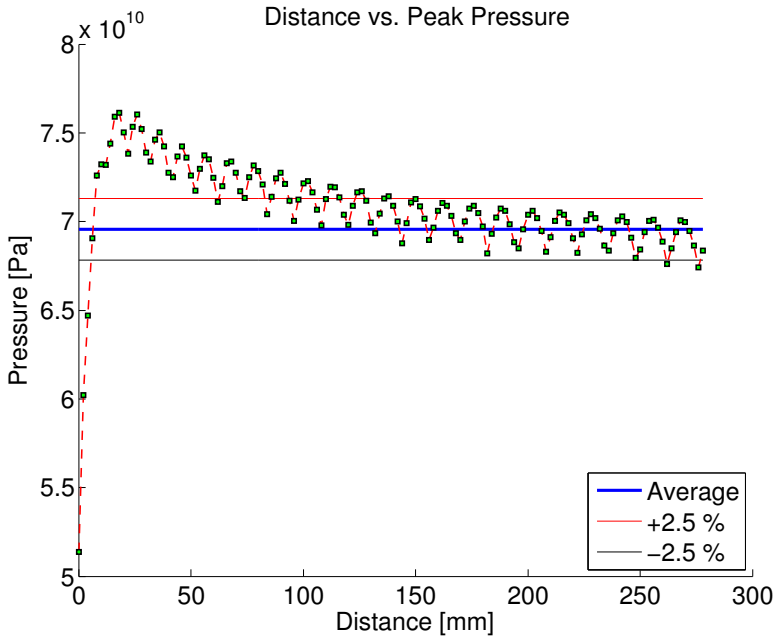


**Figure 5.15**: Distance vs. Maximum Pressure on 2mm cells Al-W layered composite.

### 5.2.3 Al-W laminate with 1mm Cells (0.5mm Layers)

In Fig. 5.16 the evolution of shock wave with the depth in laminate with cell size 1 mm is presented. From this figure we can conclude that for a relatively long time of loading pulse, determined by the thickness of the Al impactor (800 mm), the shock wave reaches a steady state, this is the only case that both composites reach a steady state behind the shock. We see oscillations of pressure behind the shock which attenuate before arrival of release wave from the free surface of impactor. Oscillations manage to disappear even at the very beginning of the composite. It is interesting that the leading part of the oscillatory shock wave and the amplitude of the leading pulse and its rise time reached in average a steady value demonstrated by 5.17 and Fig. 5.18 but contrary to the other cases, there are strong oscillations around the average value. A comparison is presented in section 6 where it is possible to see more clearly the effects that the length of the loading pulse has on the establishing of final state behind the shock.

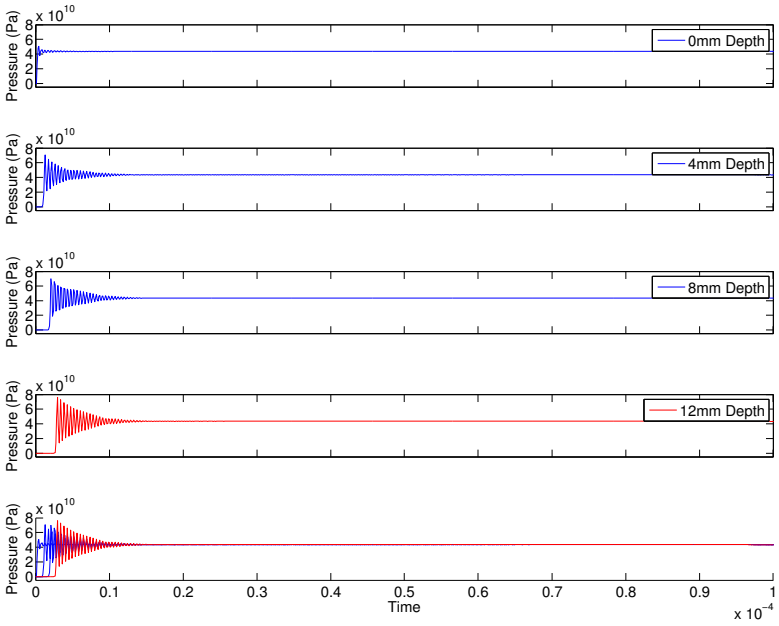


(a)

**Figure 5.16**: (a)-(d) Pressure Evolution vs. Time at different depths with 800 mm impactor and 0.5mm layers (1mm cells).

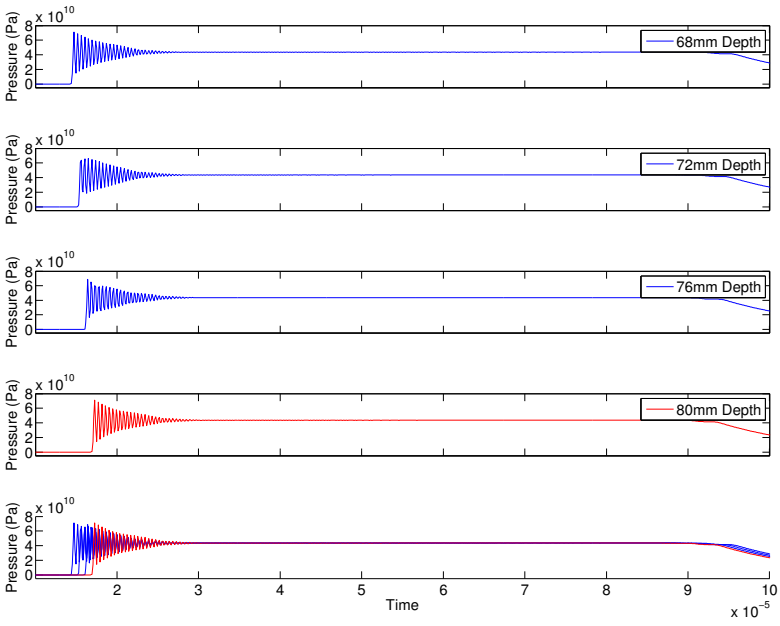


(b)

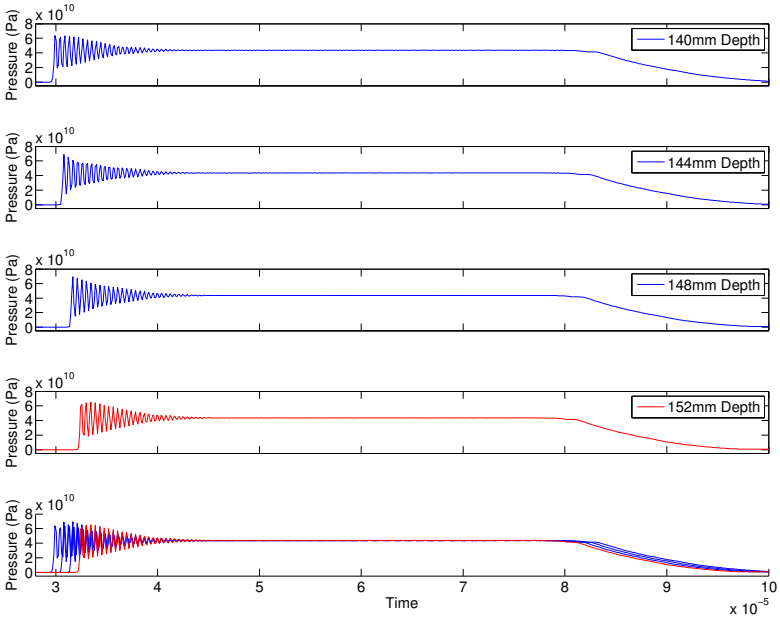


(c)

**Figure 5.16:** continued

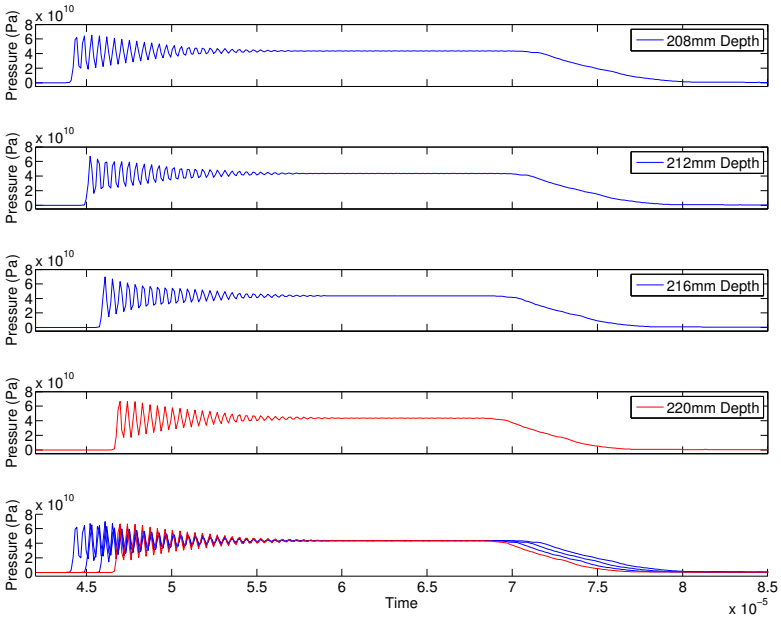


(d)

**Figure 5.16:** continued

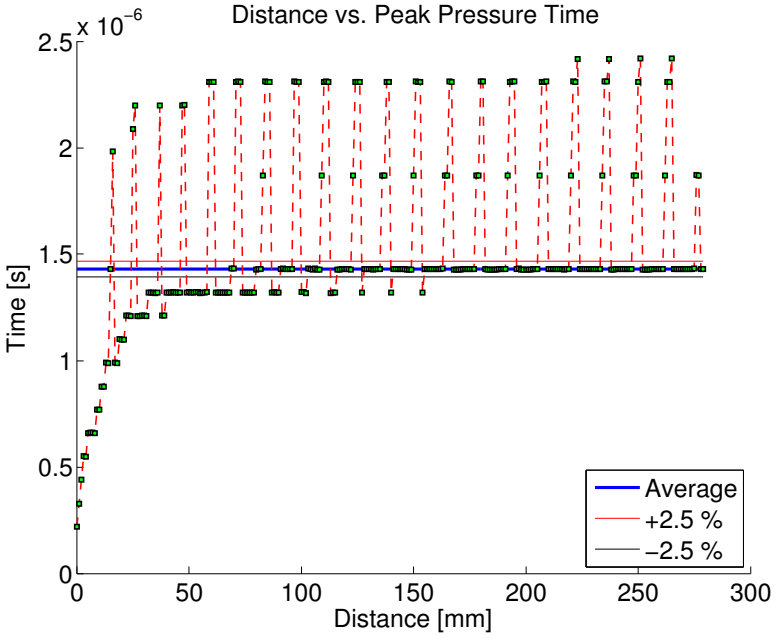


**Figure 5.17**: Distance vs. Time to maximum amplitude on a 1mm cells Al-W layered composite.

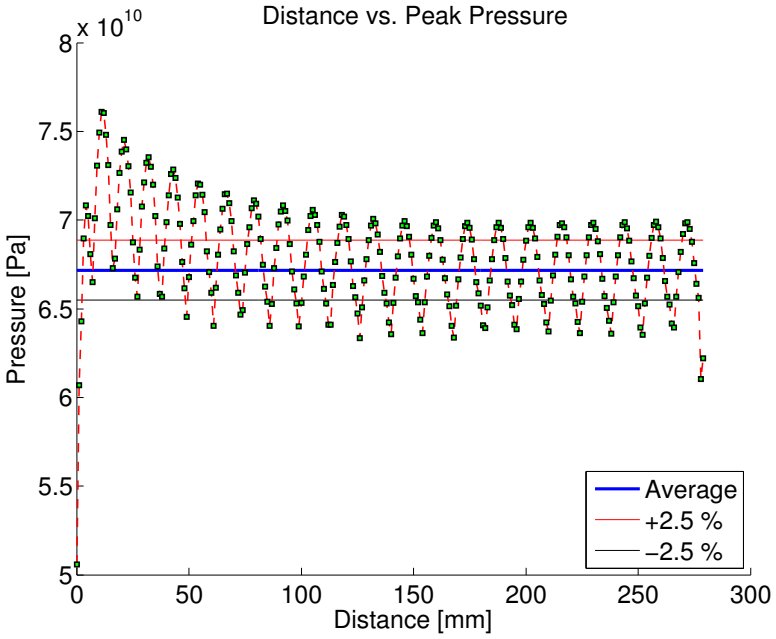


**Figure 5.18**: Distance vs. Maximum Pressure on 1mm cells Al-W layered composite.

### 5.2.4 Al-W laminate with 1mm Cells (.5mm Layers, small viscosity, mesh size)

To check a role of a smaller value of viscosity and mesh size on the dynamics of shock wave in laminates and final state we conducted calculations with reduced viscosity and mesh size. Due to memory restrictions calculations were currently conducted for 800 mm impactor and for a shock wave depth of propagation corresponding to 20 microseconds. The results are presented in Fig. 5.19 and it is possible to appreciate that the difference is almost negligible between the case with a low viscosity and a fine mesh (5.19(a)) and high viscosity coarse mesh (5.19(b))

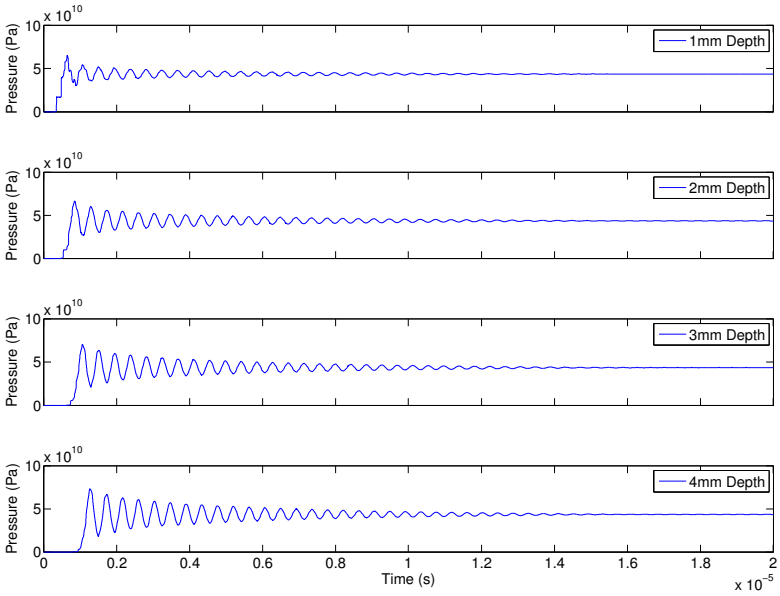


(a)

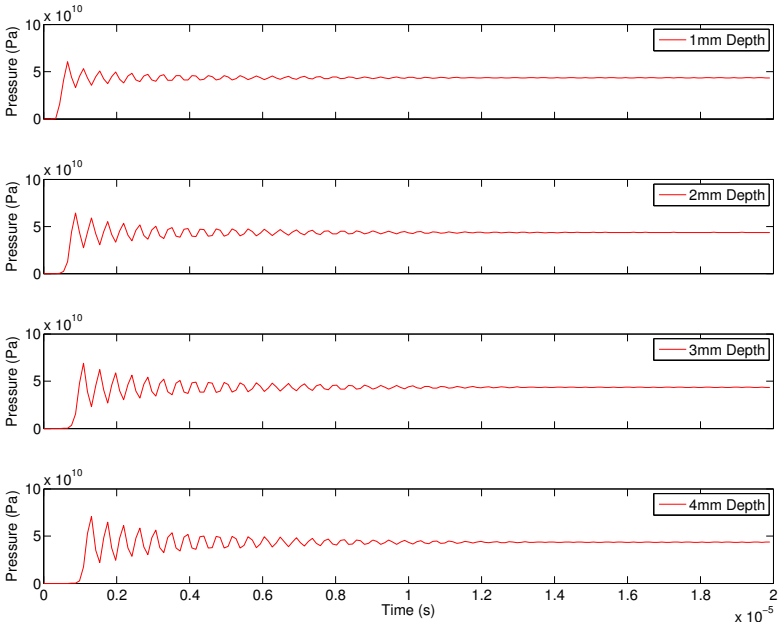


(b)

**Figure 5.19**: (a) Pressure evolution on layered material with a low viscosity and a refined mesh. (b) Pressure evolution on layered material with high viscosity and coarse mesh (same as in 5.2.3).

## 5.3 Final state of Al-W layered composite under loading by a short 80 mm impactor.

The final state of the material refers to the final pressure inside the material, specific volume and temperature behind the shock where oscillations of these parameters are negligible. In order to make a comparison with the calculated final pressure in the simulations, a Hugoniot curve for the composite material was constructed with the Isothermal Average Method and the Kinetic Energy Average Method, both presented in the Section 3.4.

For the calculation of the final equilibrium temperature in the simulations, an equilibrium temperatures of two neighboring layers of different materials composing a cell were calculated taken the same averaging procedure described in section 4.3

$$T = \frac{m_{Al} C_{P,Al} T_{Al} + m_W C_{P,W} T_W}{m_{Al} C_{P,Al} + m_W C_{P,W}}, \tag{5.1}$$

### 5.3.1 Al-W laminate with 4mm Cells (2mm Layers)

In Fig. 5.20(a-b) the final state of the material is presented. From the previous parts of this work we already know that a steady state of laminate is not reached under loading by short impactor. But it is interesting that despite pressure behind shock is close to the value predicted by models the temperature did not demonstrated similar behavior. It is important to remember that the selected models used in this work assume equilibrium state. This state in laminates can be reached only through multiple shock reverberations which are not possible under loading by short impactor and 4 mm cell size. We will see that steady sate was possible to reach under loading by short impactor for cell size 1 mm.

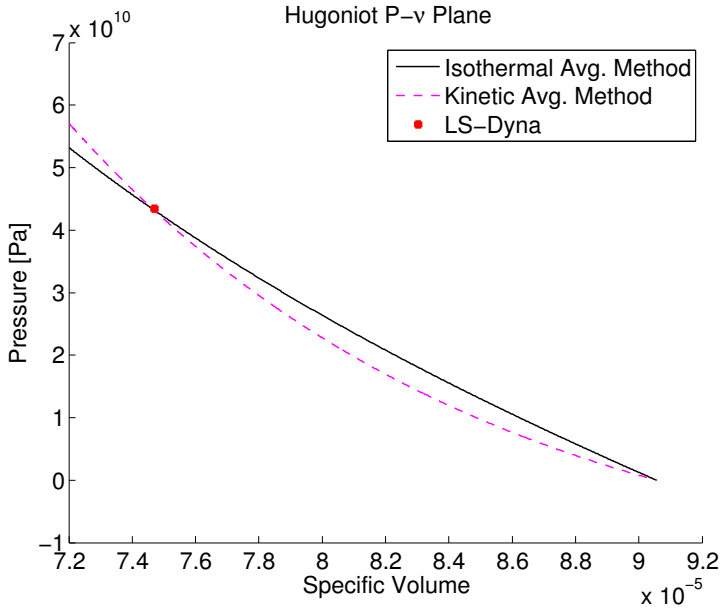


(a)

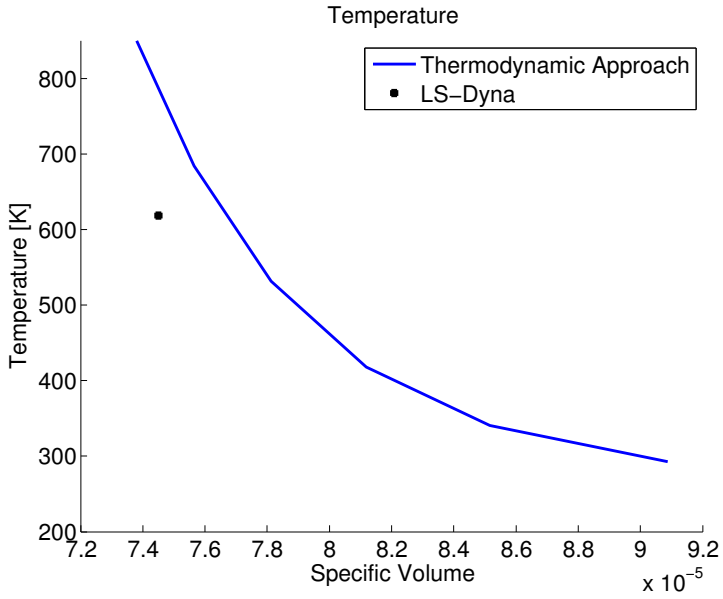


(b)

**Figure 5.20**: (a) Calculated Hugoniot based on Isothermal Averaging Method and Kinetic Energy Averaging Method vs. Simulation results (b) Calculated Temperature along the Hugoniots vs. Simulation results

### 5.3.2 Al-W laminate with 2mm Cells (1mm Layers)

In Fig. 5.21(a-b) the final state of the material is presented. In this composite, as in the previous one, the final state behind the shock was not reached. Fig. 5.21 presents the results of the comparison between the calculated Hugoniot curve and the corresponding temperature. The used approach do not correctly predict the final temperature.

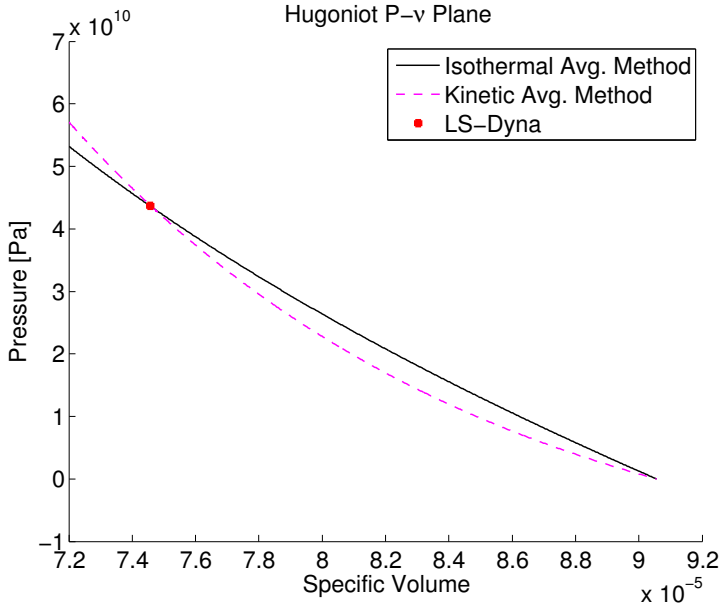


(a)

**Figure 5.21**: (a) Calculated Hugoniot based on Isothermal Averaging Method and Kinetic Energy Averaging Method vs. Simulation results (b) Calculated Temperature along the Hugoniots vs. Simulation results

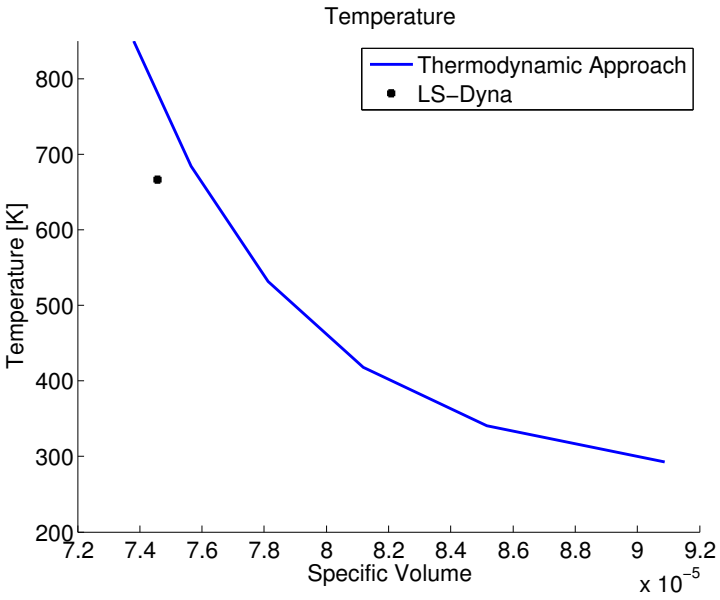


(b)

**Figure 5.21:** continued

### 5.3.3 Al-W laminate with 1mm Cells (0.5mm Layers)

In Fig. 5.22(a-b) the final state of the material is presented. In this case the lamoinates reaches a steady state. The comparison between the simulation results and the calculated Hugoniot curve as well as final temperature are in agreement with LS-Dyna calculations.

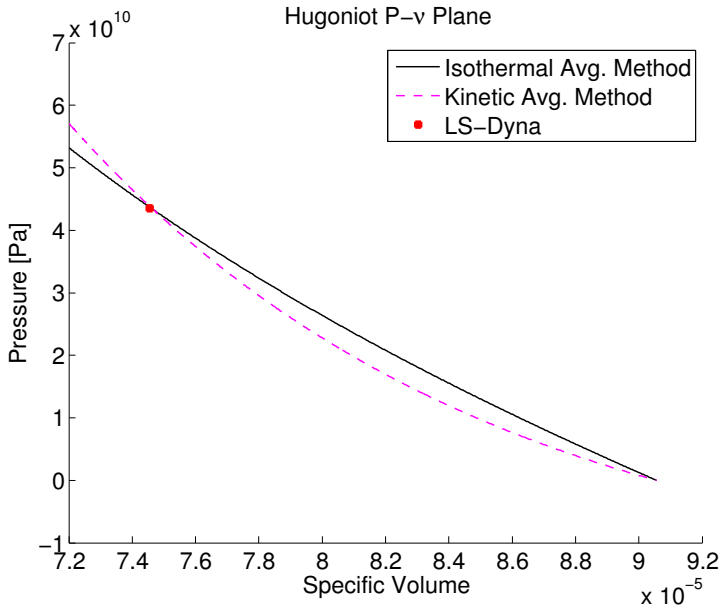


(a)

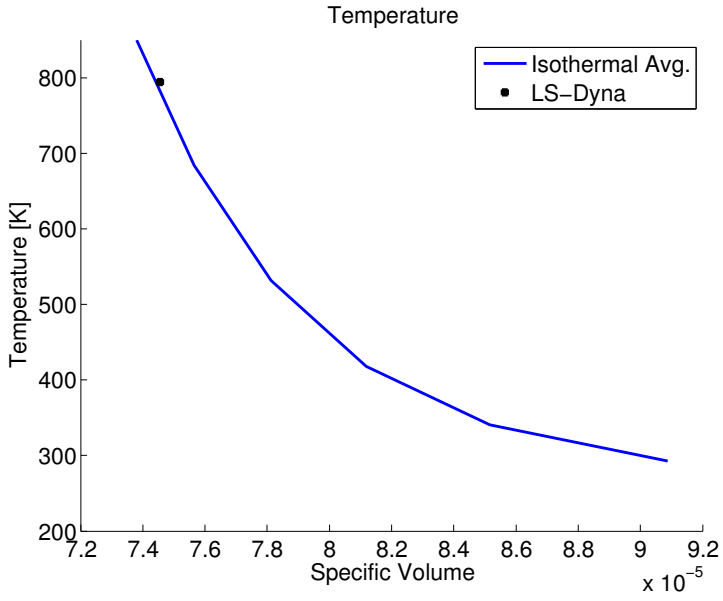


(b)

**Figure 5.22**: (a) Calculated Hugoniot based on Isothermal Averaging Method and Kinetic Energy Averaging Method vs. Simulation results (b) Calculated Temperature along the Hugoniots vs. Simulation results

## 5.4 Final state of Al-W layered composite under loading by a short 800 mm impactor.

### 5.4.1 Al-W laminate with 4mm Cells (2mm Layers)

In Fig. 5.23(a-b) the final state of the material is presented. A steady state has been reached and it can be seen the final predictions of the models are correct. It is important to make a remark on the calculated Hugoniot Curves. After the point marked as the final state on the composite, the models start to diverge from one another indicating that at least one of them might be not ideal to predict the final state behind the shock.

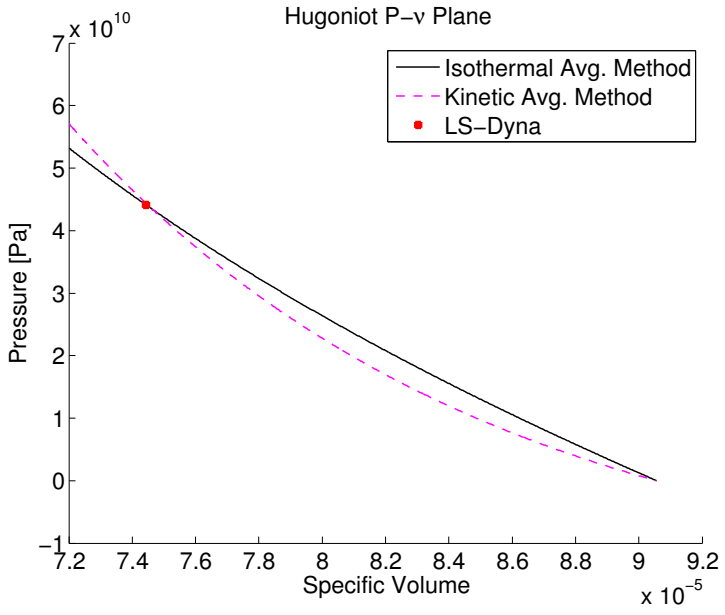


(a)

**Figure 5.23**: (a) Calculated Hugoniot based on Isothermal Averaging Method and Kinetic Energy Averaging Method vs. Simulation results (b) Calculated Temperature along the Hugoniots vs. Simulation results

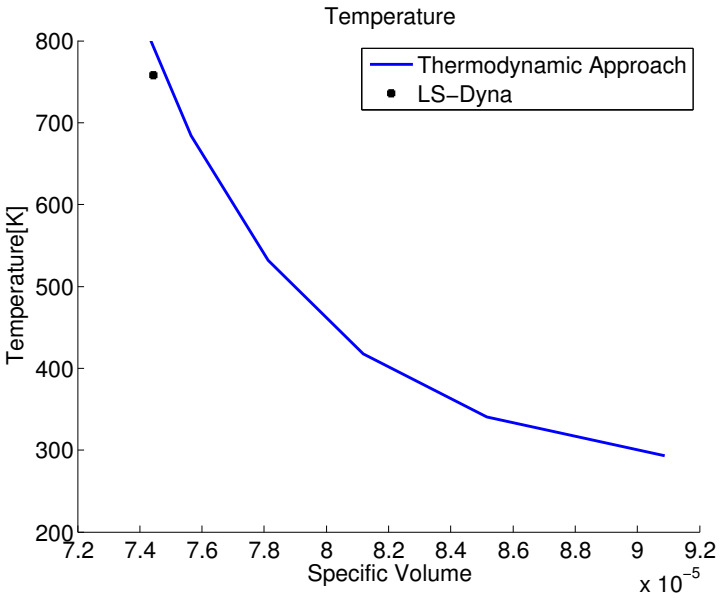


(b)

**Figure 5.23:** continued

### 5.4.2 Al-W laminate with 2mm Cells (1mm Layers)

In Fig. 5.24(a-b) the final state of the material is presented. Although it is known that this composite reached a steady state behind the traveling shock and the predicted pressure is correct, there is a difference on the temperature. The temperature calculation correctly predict the final thermodynamic state behind the shock.

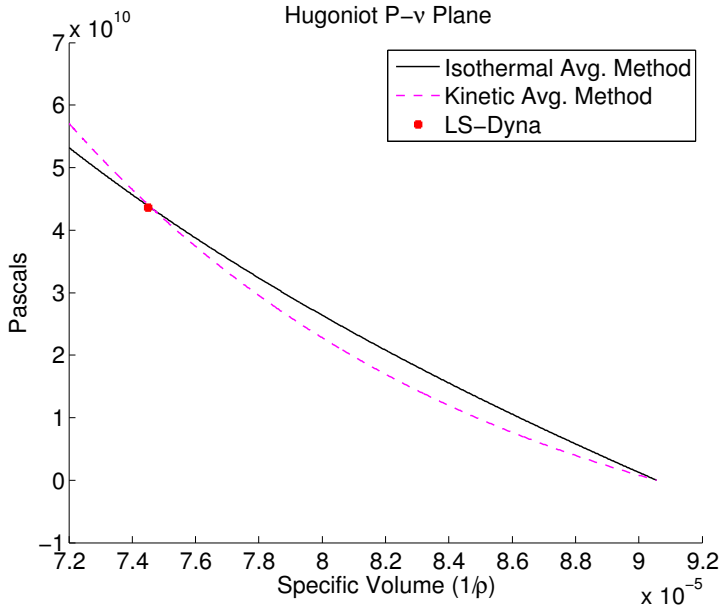


(a)

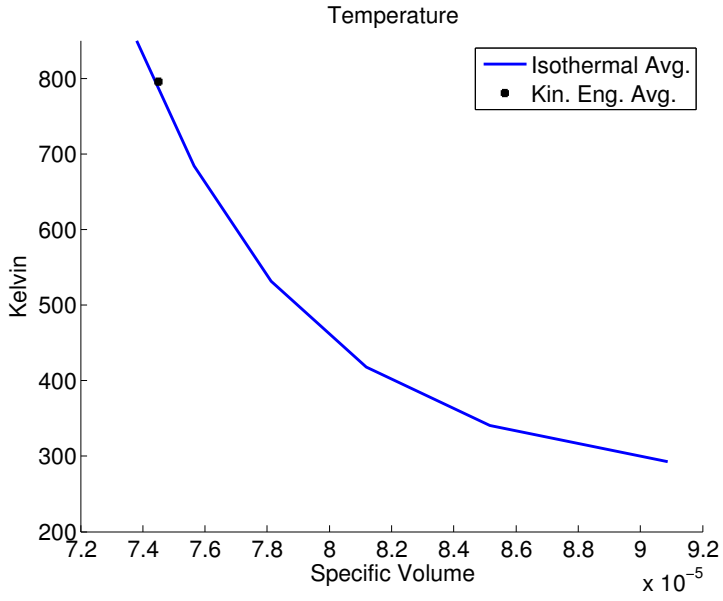


(b)

**Figure 5.24**: (a) Calculated Hugoniot based on Isothermal Averaging Method and Kinetic Energy Averaging Method vs. Simulation results (b) Calculated Temperature along the Hugoniots vs. Simulation results

### 5.4.3 Al-W laminate with 1mm Cells (0.5mm Layers)

In Fig. 5.25(a-b) the final state of the material is presented. This figure shows the same trend as the previous one, where a steady state exist and the final prediction of the final average pressure behind the shock is correct, the final temperature is correctly predicted once the shock loading process has taken place.

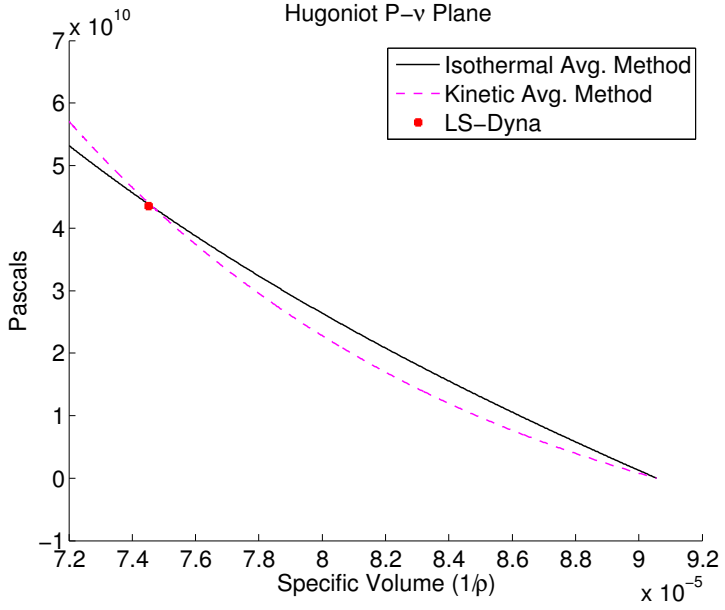


(a)

**Figure 5.25**: (a) Calculated Hugoniot based on Isothermal Averaging Method and Kinetic Energy Averaging Method vs. Simulation results (b) Calculated Temperature along the Hugoniots vs. Simulation results.

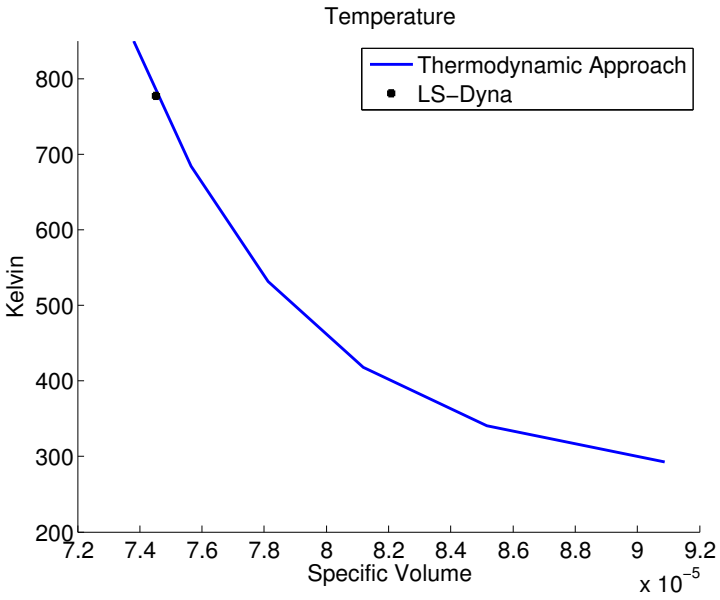


(b)

**Figure 5.25:** continued

### 5.4.4 Al-W laminate with 1mm Cells (.5mm Layers, small viscosity, mesh size)

To check a role of a smaller value of viscosity and mesh size on the dynamics of shock wave in laminates and final state we conducted calculations with reduced viscosity and mesh size. Due to memory restrictions calculations were conducted for 800 mm impactor and for a shock wave depth of propagation corresponding to 20 microseconds. The results are presented in Fig. 5.26. In this figure it is possible to appreciate that the state behind the shock reached at 20 microseconds has virtually no difference whether a low or high viscosity were used, thus implying that the final state is independent of the rise time as long as the width of the shock wave can fit inside the layer.

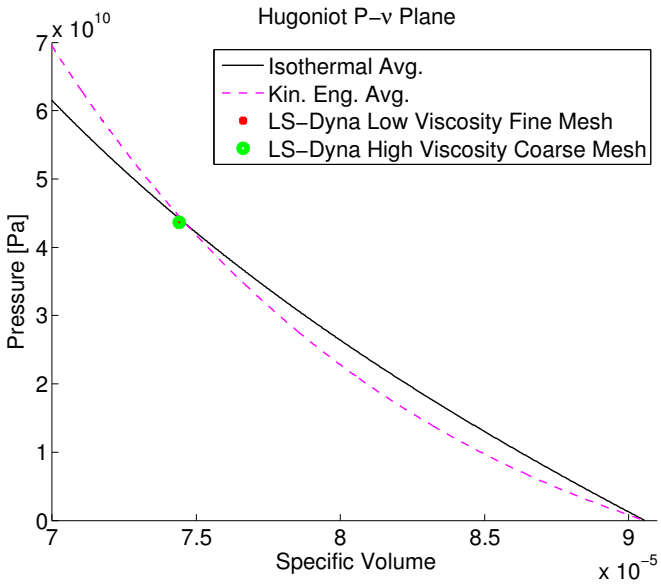


(a)

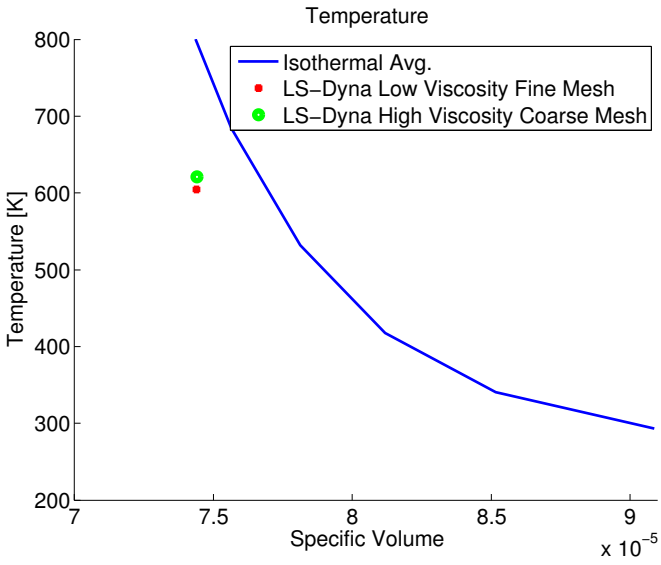


(b)

**Figure 5.26**: (a) Calculated Hugoniot based on Isothermal Averaging Method and Kinetic Energy Averaging Method vs. Simulation results with different viscosity and mesh refinement (b)Calculated Temperature along the Hugoniots vs. Simulation results with different viscosity and mesh refinement.

## 5.5 Establishment of a steady-state behind a traveling shock under the loading of short 80mm impactor.

### 5.5.1 Al-W laminate with 1mm Cells (.5mm Layers)

In Fig. 5.27 we present the time it takes the laminate to reach a steady state behind shock (where oscillations are negligible within a prescribed threshold) at different depths. From the previous sections it became clear that a steady state behind the traveling shock was only achieved in the case where the cell size in the laminate is 1mm. The set of figures demonstrates that at the 5% threshold, the rarefaction waves catches up with the front close to the middle of the composite while on the 10% threshold one, almost reaches the whole depth of the composite.

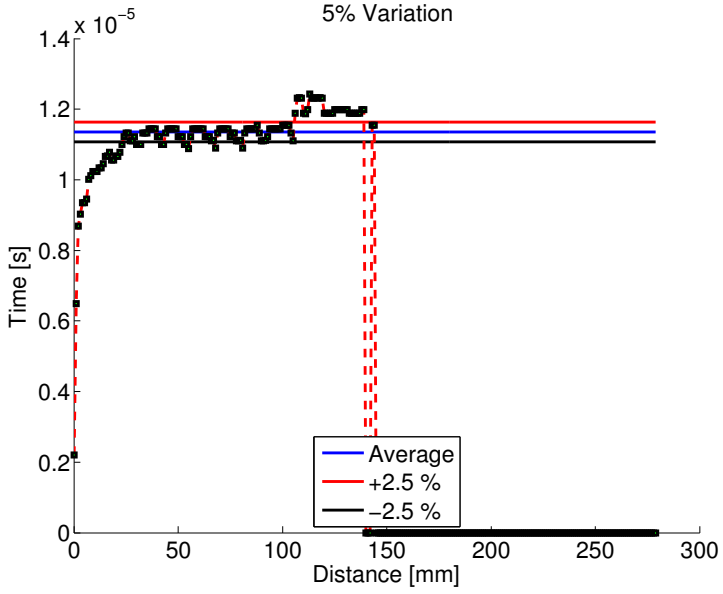


(a)

**Figure 5.27**: (a) Distance vs. Time to establish steady state with a 5% threshold. (b) Distance vs. Time to establish steady state with a 10% threshold.

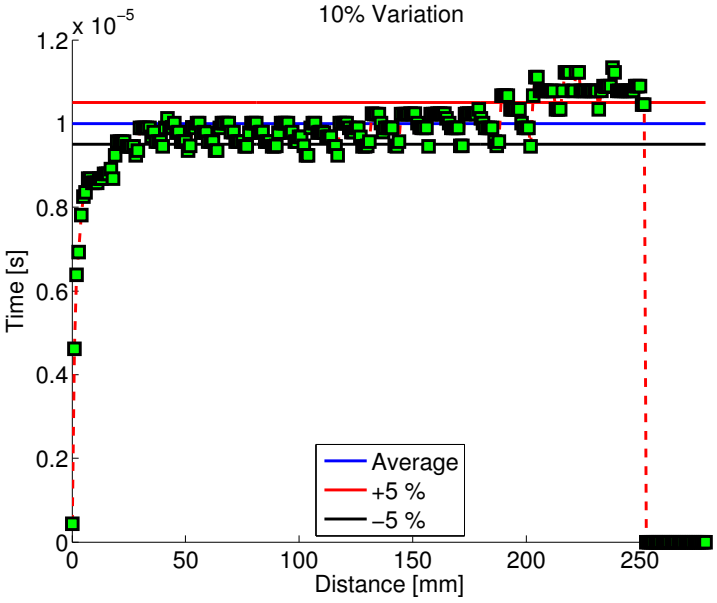


(b)

**Figure 5.27:** continued

## 5.6 Establishment of a steady-state behind a traveling shock under the loading of long 800mm impactor

On the case where the time of compression was extended by using a longer impactor (800mm) all the cases exhibit a steady state, corresponding data are presented below.

### 5.6.1 Al-W laminate with 4mm Cells (2mm Layers)

In Fig. 5.28 we present the time it takes the composite to reach a steady state behind a shock at different depths within a prescribed threshold. This happens close to the third of the depth. Also increasing the value of threshold to 10% results in establishing a steady state at shorter distances from shock entrance.

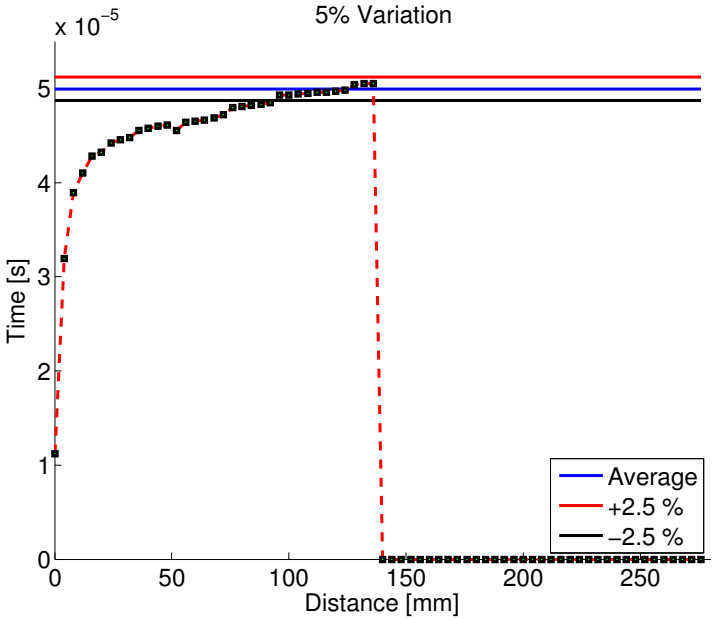


(a)

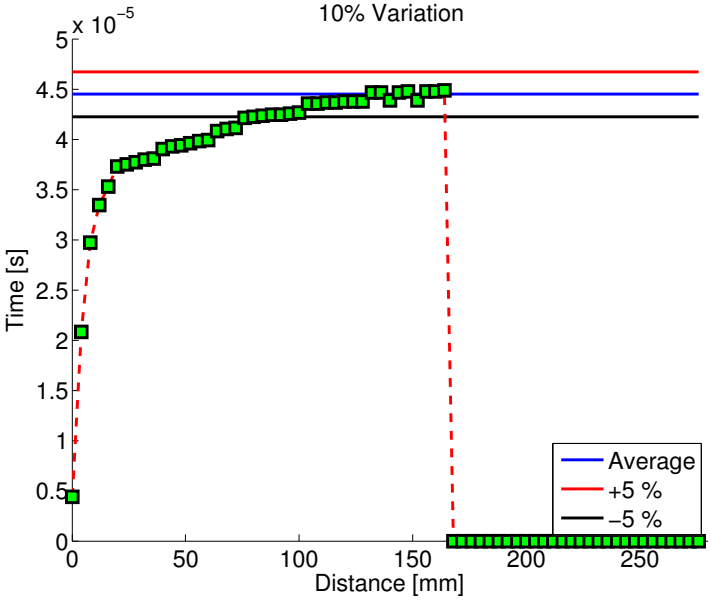


(b)

**Figure 5.28**: (a) Distance vs. Time to establish steady state with a 5% threshold. (b) Distance vs. Time to establish steady state with a 10% threshold.

### 5.6.2 Al-W laminate with 2mm Cells (1mm Layers)

In Fig. 5.29 we present the time it takes the composite to reach a steady state behind shock at different depths within a prescribed threshold. As expected, this phenomenon occurs faster (for both thresholds) than in the previous case. Fig. 5.29 supports the idea that larger number of interfaces in laminates with smaller cell size helps to achieve a steady state faster. Not only the composite reaches faster the steady state but also larger part of the composite reaches the parameters corresponding to steady state.

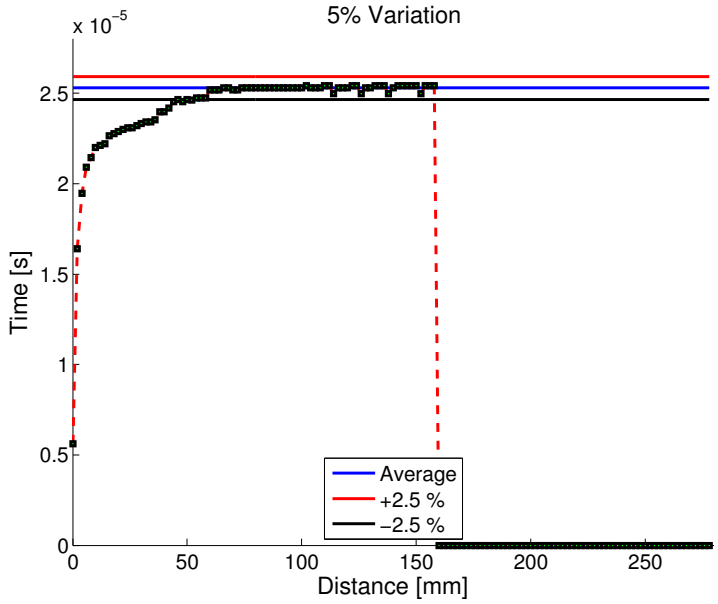


(a)

**Figure 5.29**: (a) Distance vs. Time to establish steady state with a 5% threshold. (b) Distance vs. Time to establish steady state with a 10% threshold.

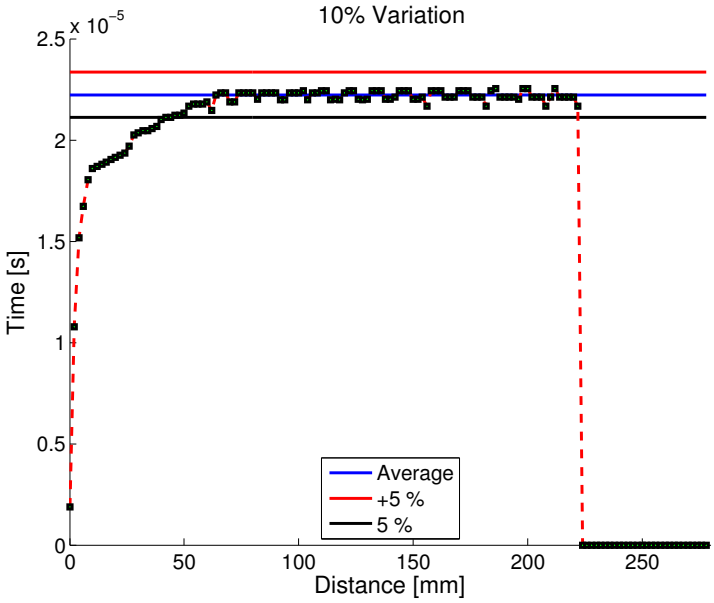


(b)

**Figure 5.29:** continued

### 5.6.3 Al-W laminate with 1mm Cells (0.5mm Layers)

In Fig. 5.30 we present the time it takes this composite to reach a steady state at different depths within a prescribed threshold. This composite with a smallest cell size is expected to reach a steady state fast. The results demonstrate how the increasing number of interfaces helps in the establishing of a steady state. From Fig. 5.29 it is easy to see that almost from the very beginning (at depth about 20mm) the steady state is reached.

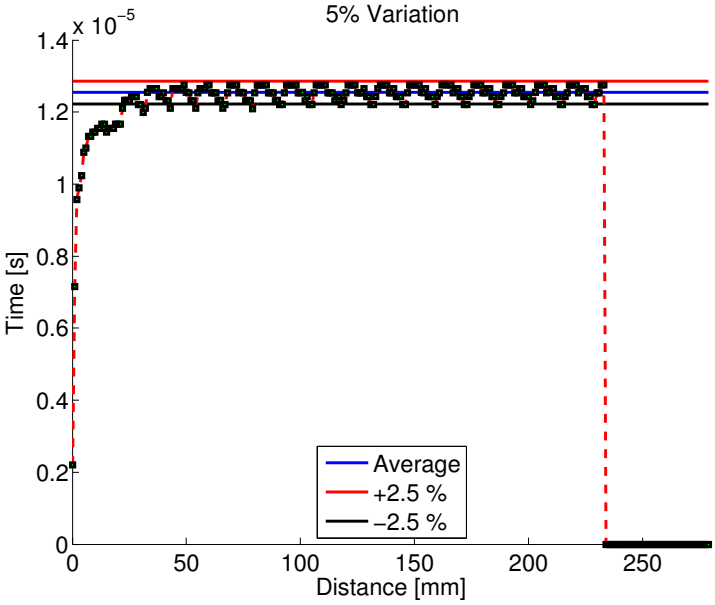


(a)

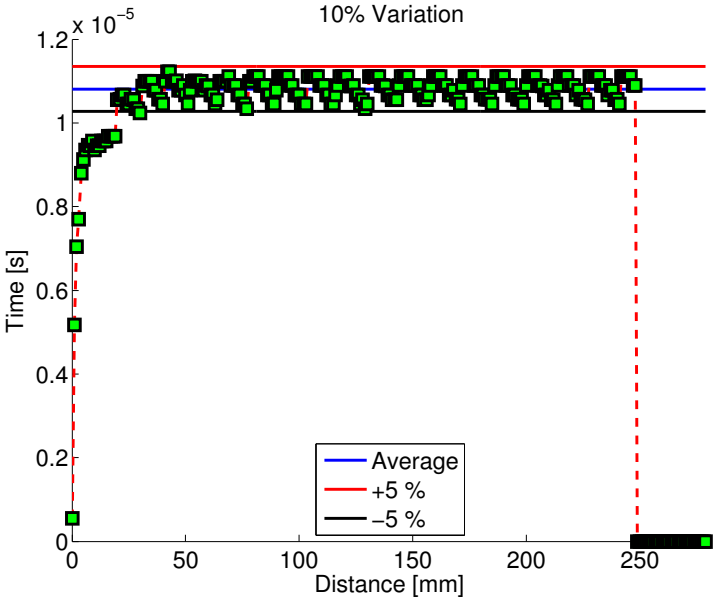


(b)

**Figure 5.30**: (a) Distance vs. Time to establish steady state with a 5% threshold. (b) Distance vs. Time to establish steady state with a 10% threshold.

Chapter 5, partially, is to be used in a subsequent publication. The thesis author is going to be the primary investigator and author of this paper.

# Chapter 6

# Conclusion

Two ad hoc models for prediction of Hugoniot curves for heterogeneous materials were analyzed using a comparison with LS-DYNA calculations of multiple shock loadings of layers representing a real path to the establishment of the final equilibrium state. The goal was to find out if these models correctly predict the final state of a shocked laminate material. Another issue was to compare the maximum pressures and temperatures achieved during the transition states of shock loading with parameters at equilibrium.

It has been demonstrated that these models (within the explored ranges of pressures) provide very good accuracy of the final average pressure in the material. Predicted Hugoniots based on corresponding models coupled with the presented thermodynamic model also give a good assessment of the final steady temperatures compared to results of LS-DYNA calculations. These calculations give an "accurate" prediction of the final temperatures of components and average temperature in the laminate because it simulates a real path of the material from initial to the final states. The maximum pressures and temperatures reached during this transient period significantly exceed the steady temperatures behind shock.

Table 6.1 presents a summary on the space and time needed to reach the steady state behind the shock. From this information, we can observe a direct relationship between time and space scales necessary for the establishment of a steady state (in situ scales) and the cell size - the main scale parameter of the initial state in laminates. This relationship is almost linear and corresponding

**Table 6.1**: Time to reach a steady state within a prescribed threshold value on different layered composites under different impactor sizes. N/A refers to a case where a steady state was never reached even within the prescribed thresholds.

| | | Length Oscillatory Tail 5% Threshold | | Length Oscillatory Tail 10% Threshold | |
|---|---|---|---|---|---|
| Layer Size [mm] | Impactor Size [mm] | Time [s] | Distance [mm] | Time [Pa] | Distance [mm] |
| 2 | 80 | N/A | N/A | N/A | N/A |
| | 800 | 4.994E-05 | 120 | 4.449E-05 | 124 |
| 1 | 80 | N/A | N/A | N/A | N/A |
| | 800 | 2.530E-05 | 60 | 2.224E-05 | 64 |
| 0.5 | 80 | 1.136E-05 | 31 | 1.000E-05 | 30 |
| | 800 | 1.254E-05 | 31 | 1.081E-05 | 31 |

scales are directly related to the cell size. It is interesting that the number of shock loading in these solid laminates required about 45 cycles to reach a steady state unlike about 10 cycles to reach a steady state in laminate material (with a solid layer/gap cell) as demonstrated by (Hofmann et al., 1968; Nesterenko, 2001). This significant difference in the number of shock reverberations may be due to the fact that energy dissipation during unloading of shocked material into gaps and subsequent additional shock loading is higher than in the corresponding cycle in a solid-solid laminate due to the larger change of pressure amplitudes during each cycle.

We can also comment on the time it takes each of the considered laminates to reach a steady shape of the leading shock front. By this we refer to the distance from the entrance to a point where the pressure rise time and the maximum pressure stop changing. It was proved that the distance and time it takes for the front of the wave to be stabilized (stop changing) has also almost linear relationship with the size of the cell, this information can be found in Table 6.2. Thus the size of the cells has also a direct effect on the distance to establish a stationary shape of the leading front.

**Table 6.2**: Time to reach peak pressure and peak pressure value on multiple layered composites under different impactor sizes

| | | Distance vs. Time to Reach Peak Pressure | | Distance vs. Peak Pressure | |
|---|---|---|---|---|---|
| Layer Size [mm] | Impactor Size [mm] | Time [s] | Distance [mm] | Pressure [Pa] | Distance [mm] |
| 2 | 80 | 5.405E-06 | 136 | 7.245E+10 | 208 |
| | 800 | 5.521E-06 | 140 | 7.254E+10 | 208 |
| 1 | 80 | 2.800E-06 | 80 | 6.956E+10 | 144 |
| | 800 | 2.798E-06 | 82 | 6.96E+10 | 142 |
| 0.5 | 80 | 1.429E-06 | 37 | 6.610E+10 | 62 |
| | 800 | 1.430E-06 | 46 | 6.718E+10 | 73 |

**Table 6.3**: Final values for pressure, temperature and specific volume after the shock loading process on different layered composites under different impactor sizes

| Layer Size [mm] | Impactor Size [mm] | Final Avg. Pressure [Pa] | Final Avg. Temperature [K] | Final Specific Volume [$m^3$/Kg] |
|---|---|---|---|---|
| 2 | 80 | 4.343E+10 | 618.3 | 7.451E-05 |
| | 800 | 4.407E+10 | 757.9 | 7.443E-05 |
| 1 | 80 | 4.368E+10 | 666.5 | 7.457E-05 |
| | 800 | 4.362E+10 | 795.9 | 7.449E-05 |
| 0.5 | 80 | 4.348E+10 | 716.9 | 7.454E-05 |
| | 800 | 4.352E+10 | 774.5 | 7.452E-05 |

The presented information demonstrated how shock waves behave inside a layered composite. Particularly it demonstrates how difficult it is to reach a steady state of the traveling shock. It also emphasizes that the analysis of shock loading in layered composites has to be handled with care since theoretical tools (like the two analyzed models) might fail to predict the real final state of the material and some counterintuitive effects may be observed especially under very short compression time.

Chapter 6, partially, is to be used in a subsequent publication. The thesis author is going to be the primary investigator and author of this paper.

# Chapter 7

# Future Work

Future work will be directed into gain a deeper understanding of shock waves on composite materials and how different mesostructure (laminates versus metal matrix composites with cylindrical inclusions) and properties of materials (e.g., porosity, interfacial bonding) could affect the final state behind the shock and mechanisms of paths to reach the final state. The work is to be conducted using finite element simulations analogous to the ones used in the present work.

We plan to add information on the final state reached under impact by a "short" impactor (8 mm) and compare results with predicted by two models and by our LS-Dyna calculations. Adding these results may be sufficient to prepare a first paper.

We will pursue a new approach with focus on understanding the effects that porosities inside the layers could have in the establishment of a steady state behind the shock and how this could affect the final state of the material. It was already demonstrated that number of shock cycles to reach a steady state is smaller in solid/solid laminates than in solid/gap laminates. Particularly we would like to compare the states at the leading front with predicted by theory (Nesterenko, 2001)

The second approach is going to be directed to understand how inclusions either in random or predetermined places affect the propagation of a shock in the layered material. These inclusions will be taken in the form of tungsten cylinders embedded into aluminum matrix (material with practical applications processed

at Nesterenko Lab at UCSD) and we plan to investigate a role of arrangements, randomness and sizes.

Another interesting phenomenon to be explored is to use these laminate materials for controlled frequency gaps with possible use for shock type disturbances. The band gap refers to a specific range of frequencies where the material acts as a band-stop filter. This particular behavior has been observed and studied for small amplitude acoustic (propagating in linear elastic materials) waves with quasiharmonic excitation. Very limited research has been conducted on shock/impact type loading which is a transient phenomena with essentially nonlinear behavior. The development of these materials may have broad applications for helmets for football players or for mitigation of impact caused by high velocity collision or explosion.

# Bibliography

J. R. Asay, L. C. Chhabildas, and D. P. Dandekar. Shear strength of shock-loaded polycrystalline tungsten. *Journal of Applied Physics*, 51(9):4774–4783, 1980.

S. S. Batsanov. *Effects of explosions on materials: modification and synthesis under high-pressure shock compression*. Springer, Berlin, November 1994.

D. J. Benson and V. F. Nesterenko. Anomalous decay of shock impulses in laminated composites. *Journal of Applied Physics*, 89(7):3622, 2001.

J. C. Crowhurst, M. R. Armstrong, K. B. Knight, J. M. Zaug, and E. M. Behymer. Invariance of the dissipative action at ultrahigh strain rates above the strong shock threshold. *Physical Review Letters*, 107(14):144302, 2011.

D. E. Grady. Structured shock waves and the fourth-power law. *Journal of Applied Physics*, 107(1):013506–013506, 2010.

J. O. Hallquist. *LS-DYNA Theory Manual*, February 2006.

R. Hofmann, D. J. Andrews, and D. E. Maxwell. Computed shock response of porous aluminum. *Journal of Applied Physics*, 39(10):4555–4562, 1968.

W. M. Isbell. *Shock waves: Measuring the dynamic response of materials*. Imperial College Pr, 2005.

R. Kinslow. *High-Velocity Impact Phenomena*. Academic Press, New York, 1st edition, 1970.

Livermore Software Technology Corporation. *LS-DYNA Keyword User's Manual Volume 1*, 971 edition, September 2012a.

Livermore Software Technology Corporation. *LS-DYNA Keyword User's Manual Volume 2*, 971 edition, September 2012b.

S. P. Marsh. *LASL Shock Hugoniot Data.* University of California Press, January 1980.

R. G. McQueen, S. P. Marsh, and J. N. Fritz. Hugoniot Equation of State of Twelve Rocks. *Journal of Geophysical Research*, 72:4999–5036, October 1967.

V. F. Nesterenko. *Dynamics of Heteregoneous Materials.* Springer, New York, 2001.

V. F. Nesterenko, V. M. Fomin, and P. A. Cheskidov. Damping of Strong Shocks in Laminar Materials. *Translated from Zhurmal Prikladnoi Mekhaniki i Teknicheskoi Fiziki*, 4:130–139, August 1983.

O. E. Petel and F. X. Jetté. Comparison of methods for calculating the shock hugoniot of mixtures. *Shock Waves*, 20(1):73–83, September 2009.

O. E. Petel, F. X. Jetté, S. Goroshin, D. L. Frost, and S. Ouellet. Blast wave attenuation through a composite of varying layer distribution. *Shock Waves*, 21 (3):215–224, January 2011.

S. M. Rytov. Acoustical Properties of a Thinly Laminated Medium. In *Electroacoustical Conference*, pages 1–13, Kiev, July 1955.

D. J. Steinberg. *Equation of State and Strength Properties of Selected Materials.* Lawrence Livermore National Laboratory, February 1996.

D. J. Steinberg, S. G. Cochran, and M. W. Guinan. A constitutive model for metals applicable at high-strain rate. *Journal of Applied Physics*, pages 1498–1504, March 1979.

S. Zhuang, G. Ravichandran, and D. E. Grady. An experimental investigation of shock wave propagation in periodically layered composites. *Journal of the Mechanics and Physics of Solids*, 51(2):245–265, 2003.